


Review

# Recent Advances in Conductive Polymers-Based Electrochemical Sensors for Biomedical and Environmental Applications

Youheng Pan <sup>1</sup>, Jing Zhang <sup>2</sup>, Xin Guo <sup>2</sup>, Yarou Li <sup>1</sup>, Lanlan Li <sup>1,\*</sup> and Lijia Pan <sup>2,\*</sup> <sup>1</sup> College of Mechanical and Electrical Engineering, Henan Agricultural University, Zhengzhou 450002, China<sup>2</sup> Collaborative Innovation Center of Advanced Microstructures, School of Electronic Science and Engineering, Nanjing University, Nanjing 210093, China

\* Correspondence: lanlan.li@henau.edu.cn (L.L.); ljpan@nju.edu.cn (L.P.)

**Abstract:** Electrochemical sensors play a pivotal role in various fields, such as biomedicine and environmental detection, due to their exceptional sensitivity, selectivity, stability, rapid response time, user-friendly operation, and ease of miniaturization and integration. In addition to the research conducted in the application field, significant focus is placed on the selection and optimization of electrode interface materials for electrochemical sensors. The detection performance of these sensors can be significantly enhanced by modifying the interface of either inorganic metal electrodes or printed electrodes. Among numerous available modification materials, conductive polymers (CPs) possess not only excellent conductivity exhibited by inorganic conductors but also unique three-dimensional structural characteristics inherent to polymers. This distinctive combination allows CPs to increase active sites during the detection process while providing channels for rapid ion transmission and facilitating efficient electron transfer during reaction processes. This review article primarily highlights recent research progress concerning CPs as an ideal choice for modifying electrochemical sensors owing to their remarkable features that make them well-suited for biomedical and environmental applications.

**Keywords:** conductive polymers; electrochemical sensor; biomedical application; environmental application



**Citation:** Pan, Y.; Zhang, J.; Guo, X.; Li, Y.; Li, L.; Pan, L. Recent Advances in Conductive Polymers-Based Electrochemical Sensors for Biomedical and Environmental Applications. *Polymers* **2024**, *16*, 1597. <https://doi.org/10.3390/polym16111597>

Academic Editor: Chi-Jung Chang

Received: 1 April 2024

Revised: 27 May 2024

Accepted: 30 May 2024

Published: 4 June 2024



**Copyright:** © 2024 by the authors. Licensee MDPI, Basel, Switzerland. This article is an open access article distributed under the terms and conditions of the Creative Commons Attribution (CC BY) license (<https://creativecommons.org/licenses/by/4.0/>).

## 1. Introduction

### 1.1. Electrochemical Sensor

Electrochemical sensor is a device that utilizes electrochemical principles for the detection of specific chemical substances, and it can be categorized into various types based on their distinct operational principles and application domains. The pH sensors are utilized for the measurement of solution pH [1–3]. Biosensors employ biological materials, such as enzymes or antibodies, as recognition elements to detect metabolites or monitor growth state [4–7]. Gas sensors are employed for the detection of gas concentration [8,9]. Ion-selective electrodes are utilized for the detection of specific ion concentrations [10]. Compared to colorimetric, fluorescent, and other sensors, electrochemical sensors provide fast reaction, high sensitivity, ease of operation, and miniaturization. Furthermore, real-time detection is possible when paired with microchannel technology. Compared to many electrochemical sensor research studies, the forms of commercialization are significantly lower. The most prevalent commercial electrochemical sensors should be blood glucose meters, which can assist patients in understanding their blood glucose levels more quickly. Furthermore, commercial electrochemical sensors include gas sensors for ammonia, formaldehyde, and oxygen, as well as ion-selective electrodes for pH, nitrate, and potassium plasma in water. Commercial applications are restricted, owing to the drawbacks of electrochemical sensors. Firstly, there is a high reliance on environmental factors. Environmental factors such as humidity, air pressure, and temperature all have an impact on electrochemical sensor performance. For example, increasing humidity causes

decreased oxygen permeability and sensor performance. Air pressure fluctuations can potentially have an effect on electrochemical process stability. At high temperatures, the electrochemical sensor's REDOX reaction rate accelerates, whereas at low temperatures it slows down. Because electrochemical sensors are extremely sensitive to temperature, they are typically temperature adjusted internally to keep the temperature as steady as feasible. Secondly, various factors in complicated environments can interfere with electrochemical sensors, reducing their accuracy and dependability. Furthermore, the electricity of electrochemical sensors is particularly susceptible to pollution and corrosion, which reduces their sensitivity and reaction time. In practical applications, electrodes must be cleaned and maintained on a regular basis to ensure proper operation. All of these facts affect the accuracy and dependability of the electrochemical sensor, limiting its commercial usage. To mitigate these effects while using an electrochemical sensor, the testing environment must be stable. Furthermore, electrochemical sensors must be calibrated while in use to ensure accurate and consistent measurement findings. Calibration is the process of comparing a sensor's response to a known standard or reference material. The specific calibration techniques vary depending on the sensor type and target analyte. Calibration is normally achieved by creating a reference solution with a known concentration of an analyte and testing the sensor's response under controlled conditions. Standard calibration materials are often certified reference materials (CRMs) or standard reference materials (SRMs) issued by a certified agency, such as the National Institute of Standards and Technology (NIST). Furthermore, numerous studies aim to enhance the anti-interference capabilities of electrochemical sensors. Selective membranes, for instance, have been employed to lessen chemical influence. To mitigate the effects of the aforementioned factors on sensor performance as much as possible, a variety of nanomaterials with environmental stability and particular recognition properties are used to further modify the electrode.

The typical configuration of an electrochemical sensor comprises a working electrode (WE), a reference electrode (RE), and a counter electrode (CE) [11]. The WE serves as the electrode that undergoes electrochemical reactions with the substance to be detected, while the RE is utilized to provide a stable potential reference, and the CE is employed for current measurement. The research on electrochemical sensors primarily focuses on two key aspects: identifying a suitable recognition element for specific substance detection and enhancing the working electrode interface through nanomaterial modifications. The recognition element plays a crucial role in the specific identification of electrochemical sensors and can effectively improve the anti-interference of the sensor. Furthermore, it is of paramount importance to conduct further research on materials for modifying the WE interface. Typically, the WE is an inorganic metal electrode or a printed electrode, and employing nanomaterials for modification not only expands the planar electrode into three dimensions but also significantly increases its specific surface area. This provides ample sites for high-density loading of recognition elements and greatly enhances the likelihood of electrochemical reactions occurring on the electrode surface. Additionally, due to their excellent conductivity, nanomaterials facilitate rapid recording of reaction signals by providing efficient electron transfer pathways during the reaction process. Commonly utilized modified nanomaterials comprise of nanoparticles, carbon nanotubes, molecularly imprinted polymers, or conductive polymers [12–18].

### 1.2. Conductive Polymers

Polymers generally refer to compounds composed of polymer chains, which typically exhibit relative molecular weights ranging from several thousand to several million. The electrical conductivity of both natural and synthetic polymers was initially extremely poor, with significant advancements in the synthesis of conductive polymers (CPs) not occurring until the 1970s [19]. The distinguishing feature of CPs lies in the presence of a conjugated main electron system, enabling them to be doped for achieving conductivity levels surpassing  $1000 \text{ S}\cdot\text{cm}^{-1}$ . These materials demonstrate conductivity during oxidation (positive doping or p-doping) or reduction (negative doping or n-doping), which can be attributed to the

presence of alternating single and multiple bonds (double or triple bonds) as illustrated in Figure 1. The  $\pi$  electrons associated with multiple bonds are delocalized throughout the extended region of the conjugated structure, rendering the polymer susceptible to oxidation or reduction through doping processes. The doping of  $\pi$ -conjugated systems reduces structural and morphological disorder, thereby enhancing conductivity from the interface between insulating materials and semiconductors towards metallic behavior, often resulting in an increased level of conductivity [20,21]. The conductivity of CPs in their neutral state typically ranges from  $10^{-6}$  to  $10^{-10}$  S·cm $^{-1}$ , but can reach values up to  $10^5$  when doped.

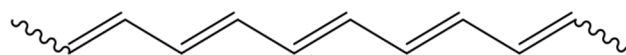


**Figure 1.** Structure of polyacetylene, showing the main chain containing conjugated double bonds.

The synthesis of CPs can be achieved through various methods. The most commonly employed synthetic principle is oxidative coupling, which involves the oxidation of monomers to generate cationic free radicals that subsequently undergo coupling reactions to form cations, leading to polymer formation in a repetitive manner. Due to its simplicity and reproducibility, electrochemical synthesis has become the favored and widely accepted approach for fabricating CPs. Another advantageous feature of electrochemical polymerization lies in its ability to operate at room temperature, while allowing precise control over the thickness of thin films through manipulation of potential or current profiles. The electrochemical polymerization of CPs typically employs one of these approaches: (1) constant current or constant current density; (2) constant potential or fixed voltage; (3) potential scanning/cycling or cyclic voltammetry techniques. Commonly used anode materials include chromium, gold, nickel, palladium, and titanium platinum-coated electrodes, as well as indium tin oxide-coated glass plates. Additionally, semiconductor materials such as n-doped silicon [22], cadmium sulfide [23] and semi-metallic graphite [24] are employed for the electrochemical growth of CPs films. This synthetic approach enables the preparation of independent, homogeneous, self-doped thin films while also allowing for copolymerization and grafting reactions to occur if desired.

CPs have many excellent properties, such as electrical conductivity, flexibility, chemical stability, optical transparency, mechanical strength, thermal stability, and biocompatibility. These properties make CPs have wide application potential in flexible electronic devices, sensors, optoelectronic devices, biomedical devices, anti-static materials and so on. At the same time, the structure of CPs can achieve specific performance requirements by regulating the chemical composition and structure of the polymer, making it suitable for different application fields (Figure 2).



**Figure 2.** CPs are widely used in various fields because of their many characteristics.

### 1.2.1. Polypyrrole(PPy)

The basic structure of PPy comprises recurring pyrrole units, which encompass nitrogen atoms and benzene rings in their chemical composition (Figure 3). These pyrrole units are interconnected through conjugated structures, giving rise to polymer chains with conductive properties. PPy stands out among various CPs due to its readily oxidizable monomer, water solubility, commercial availability, lightweight nature, affordability, and biocompatibility [25]. Moreover, PPy demonstrates exceptional conductivity, flexibility, environmental stability, and redox properties. Consequently, it has been widely employed in various biochemical and electrochemical devices [26–28]. The combination of PPy with other materials such as carbon-based materials and metal oxides enables the formation of composite materials that exhibit higher electrical conductivity and larger specific surface area. These unique characteristics make PPy an ideal candidate to meet the requirements of electrochemical sensor equipment.

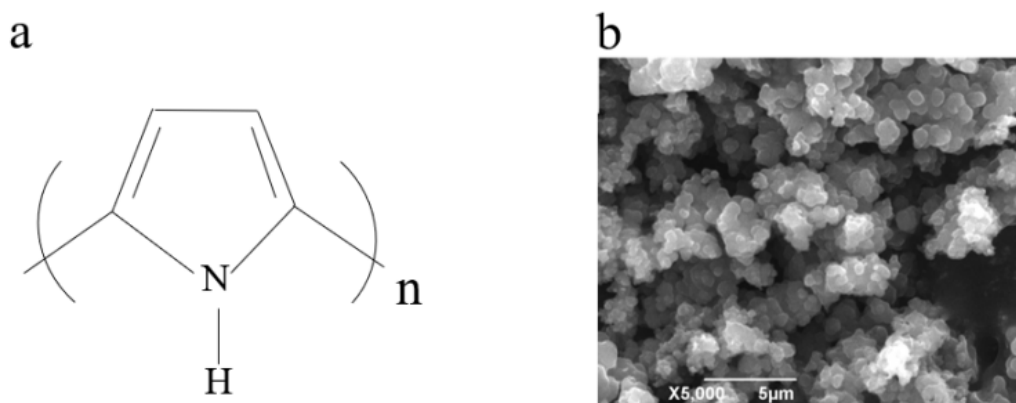


**Figure 3.** (a) Chemical structure diagram of PPy. (b) SEM image of PPy. Reprinted with permission from ref. [29].

### 1.2.2. Polyaniline(PANI)

The exceptional environmental stability, high processability, adjustable electrical conductivity and optical properties render PANI as one of the most promising conjugated CPs [30]. The widely accepted structural formula for conductive PANI, proposed by MacDiarmid in 1987, is based on the co-existence model of a “benzene-benzene” chain reduction unit and a “benzene-quinone” alternating oxidation unit, as depicted in Figure 4a. PANI exhibits distinct oxidation states, colors, and electrical conductivity based on the composition of these two structural units, which can interconvert. Since conjugated polymer compounds readily undergo REDOX reactions, PANI can be doped through electrochemical or chemical methods to neutralize the embedded ions in the polymer skeleton and the charge on the polymeric main chain. This enables PANI to rapidly and reversibly transition from an insulating state to a conductive state. When protonic acid is used for doping PANI, the imine nitrogen atom on the molecular chain undergoes protonation reaction under the influence of protonic acid, leading to delocalization and migration of positive charges onto the linear conjugate structure [31]. As a result, PANI exhibits excellent conductivity and unique three-dimensional (3D) crosslinking structure (Figure 4b,c).

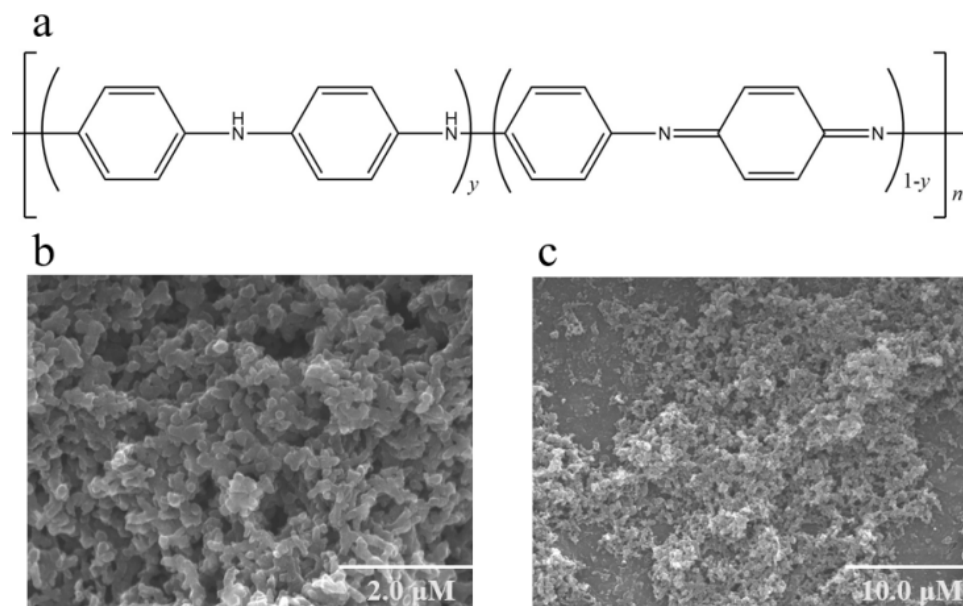


**Figure 4.** (a) Chemical structure diagram of PANI. (b,c) SEM images of PANI with different scales. Reprinted with permission from ref. [32].

### 1.2.3. Polythiophene(PTh)

PTh, along with its undoped state and derivatives, has garnered significant attention in the field of sensor applications due to its discerning barrier characteristics towards specific molecules and high affinity for adsorption [33]. The electronic properties of PTh can be modulated by the introduction of side chain groups or the addition of dopants with band gaps ranging from three electron volts to one [34]. The polymerization and deposition of PTh on large insulating substrates, however, present significant challenges due to their high oxidation potential. Moreover, the oxidized state of doping is highly unstable in air and quickly reverts back to its intrinsic state. Several methods can be employed for preparing polymer films, including solution chemical oxidation, electrochemical oxidation, oxidative chemical vapor deposition, and electrospinning [35–37]. The exceptional electrical conductivity, thermal conductivity, and processing stability of P3ATs make them highly regarded as one of the most important types of PTh, such as poly(3-hexylthiophene) (P3HT), poly(3-amylthiophene) (P3PT), and poly(3-butylthiophene) (P3BT) [38,39]. The increase in alkyl chain length within these polymer structures results in a gradual enhancement of phase separation degree, thereby leading to an improved balance between hole and electron transport [40–42]. Figure 5 shows the chemical structure diagram and SEM characterization of PTh.

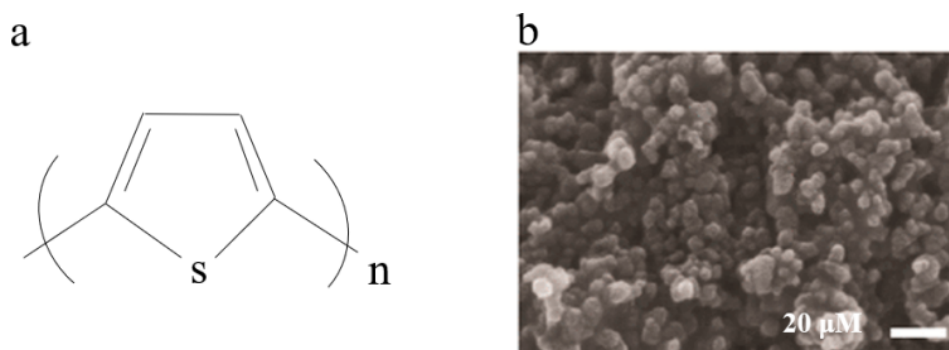


**Figure 5.** (a) Chemical structure diagram of PTh. (b) SEM image of PTh. Reprinted with permission from ref. [43].

#### 1.2.4. Poly (3, 4-acetylene dioxthiophene) (PEDOT)

PEDOT is a conjugated polymer that achieves charge conduction through a system of conjugated  $\pi$  electrons; it also exhibits excellent electrical conductivity and solubility due to its chemical structure consisting of acetylene dioxthiophene units that form polymer chains through polymerization (Figure 6). Furthermore, it can be compounded with other materials to enhance its properties and adapt to specific application requirements. For instance, hydrophilic surfactants like polystyrene sulfonate (PSS) are often incorporated to improve the water processability of PEDOT film. The combination of PSS and PEDOT results in the formation of a water-soluble PEDOT/PSS mixture [44,45]. Various methods have been employed to improve the conductivity of PEDOT/PSS, such as using polar solvents (e.g., dimethyl sulfoxide, ethylene glycol, and cosolvents [46]) or acids (e.g., chloroplatinic acid, sulfonic acid, and inorganic acid [47–49]) to eliminate excessive PSS and induce phase separation or morphological rearrangement. The recent advancement in electrospinning technology has enabled the preparation of flexible conductive PEDOT/PSS nanofibers [50].

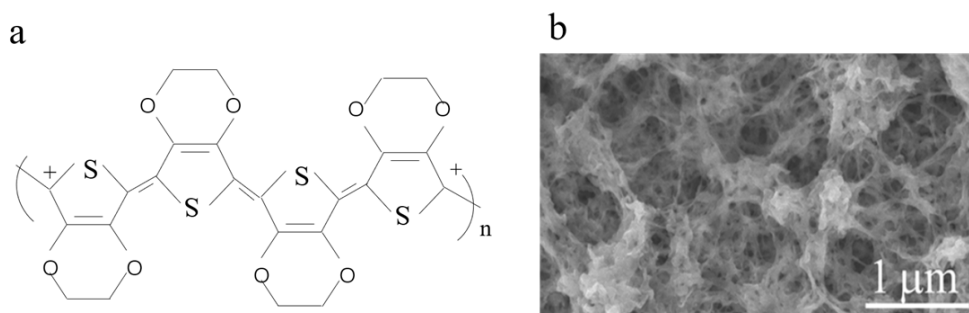


**Figure 6.** (a) Chemical structure diagram of PEDOT. (b) SEM image of PEDOT. Reprinted with permission from ref. [51].

#### 1.2.5. Polyacetylene (PA)

PA is a linear conjugated polymer composed of a polyene chain. Being one of the most fundamental organic polymers, the conductivity of PA is significantly influenced by its conformation [52]. Cis-polyacetylene and trans-polyacetylene exhibit conductivities of  $10^{-9} \text{ S}\cdot\text{cm}^{-1}$  and  $10^{-6} \text{ S}\cdot\text{cm}^{-1}$ , respectively [53]. However, the conductivity of PA can approach metallic levels ( $10^4$ – $10^5 \text{ S}\cdot\text{cm}^{-1}$ ) through p- or n-doping processes [54–56]. The practical applications of PA are limited due to its high instability and challenging processing characteristics [57,58]. The methods employed for the preparation of PA encompass catalytic polymerization, non-catalytic polymerization, and precursor-assisted synthesis [59]. Catalytic polymerization techniques are commonly used to produce PA or oligomers, necessitating catalysts with high solubility and selectivity. Radiative polymerization methods, such as glow discharge, ultraviolet or gamma rays, can also be employed to synthesize PA without the need of catalysts or solvents, thereby exhibiting significant potential for future advancements in this field. To improve the conductivity properties, PA is often hybridized or doped with other materials, such as hexamethylene phosphate, quaternary ammonium salt cellulose nanoparticles or gold nanoparticles [60–62]. Subsequently, it can be employed in electrochemical biosensors and bioelectrodes.

#### 1.2.6. Poly(p-phenylene vinylene) (PPV)

The chemical structure of PPV consists of a benzene ring and ethylene monomer, where the benzene ring is connected by conjugated double bonds to form a conjugated  $\pi$ -electron system [63]. The molecular structure of PPV contains a large number of  $\pi$ -conjugated bonds, which form a conjugated system that allows electrons to move freely throughout the entire molecule. The conjugated structure enables electrons to efficiently conduct within the polymer chain, resulting in a higher conductivity of the polymer. Moreover, the planar

arrangement of PPV facilitates the movement of electrons between molecules, promotes the formation of conjugated structures, and thus improves conductivity. The introduction of additional charge carriers through doping can further enhance the conductivity, while the redox reaction affects its conductivity, which can be adjusted by control [64]. These characteristics make PPV have broad application prospects in fields such as optoelectronic devices and organic light-emitting diodes (OLEDs).

There are numerous varieties of CPs, and we just provide a quick overview of the most widely used ones. In this review, we will look at the biological and environmental applications of these CPs-based electrochemical sensors. Additionally, we analyze the composite methods of CPs with other materials, as well as their structural characteristics, advantages, and exceptional features in sensor technology. This distinctive combination allows CPs to increase active sites during the detection process while providing channels for rapid ion transmission and facilitating efficient electron transfer during reaction processes. The methods for CPs to enhance the active sites during detection include surface chemical modification, nanocomposite, biological fixation, and electrochemical methods. The surface of CPs is chemically modified to introduce active or functional groups, such as carboxyl, amino, hydroxyl, etc. These functional groups can provide active sites, enhance the interaction with the molecules to be measured, and thus improve the sensitivity and selectivity of the sensor. Nanocomposites are formed by combining nanomaterials with conductive polymers. Commonly used nanomaterials include gold nanoparticles, carbon nanotubes, and nano-oxides. These nanomaterials have large specific surface area and special electronic structure, which form additional active sites on the CPs surface and enhance the interaction with the target molecules. Biomolecules (such as enzymes, antibodies, DNA, etc.) are fixed on the CPs surface to construct biosensors. These biomolecules have the ability to specifically recognize target molecules, and when combined with CPs, the biometric recognition performance of the sensor can be enhanced. The active sites were formed on the CPs surface by electrochemical method. For example, electrochemical techniques such as cyclic voltammetry and amperometry can be used to control the REDOX reaction on the surface of CPs to form an active site and enhance its ability to interact with target molecules. These methods can be used individually or in combination to improve the performance of the sensor and achieve highly sensitive and selective detection of the target molecule. Our aim is to showcase the latest advancements in materials science concerning sustainability, scalability, long-term stability, and cost-effectiveness while exploring future directions for polymer synthesis and utilization. These innovative materials hold promise for addressing pressing issues across various fields such as biomedicine and rapid environmental monitoring.

## 2. Biomedical Applications

Electrochemical sensors based on CPs have a wide range of applications in the biomedical field, including biomolecular detection, identification of cancer markers, and drug screening and delivery. These sensors not only enable highly sensitive and selective detection of target molecules in biological samples but also play a crucial role in precise drug release, cell status monitoring, and artificial organ research and development. As such, they significantly contribute to the advancement of biomedical science and clinical medicine.

### 2.1. Biomolecular Detection

#### 2.1.1. pH

The pH level has a significant impact on the human body and plays a crucial role in maintaining the stability and proper functioning of the internal environment. The optimal blood pH ranges from 7.35 to 7.45, and even slight deviations can lead to severe physiological issues [65]. Imbalances in pH, either too alkaline or too acidic, can negatively affect protein function, enzyme activity, metabolism, and cellular processes [66]. The digestive system also relies on specific pH levels for different functions. For instance, stomach acid with a pH of approximately 1–2 aids in food digestion and pathogen elimination [67].

Conversely, the small intestine requires a relatively alkaline environment (around 8) to facilitate enzyme activity and nutrient absorption [68]. The pH of the intracellular and extracellular environments plays a critical role in cell function and metabolic processes. Different cells and tissues have distinct requirements for specific pH ranges, which are essential for maintaining cell membrane stability, regulating enzyme activity, and facilitating ion channel function [69]. In summary, maintaining proper pH levels is crucial for the optimal functioning of the human body's physiological properties. Consequently, there arises a pressing need to develop a portable device capable of swiftly and accurately detecting pH levels. Electrochemical sensors based on CPs have emerged as the preferred choice owing to their exceptional conductivity, expansive surface area, and selectivity.

There are two types of sensors for real-time pH monitoring: *in vivo* and *in vitro*. When measuring pH within the body, most researchers opt to measure it through the design and preparation of microneedles that can be inserted into the skin. The development of a manganese-based potential sensor utilizing 3D-printed hollow microneedles (HMNs) is demonstrated by Parrilla (Figure 7a,b) [70]. The 3D-printed microneedle patch was inserted into pig skin using a quasi-membrane model, and its piercing capability was verified. The hollow nanoparticles were subsequently filled with conductive ink to fabricate a set of microelectrodes. Additionally, the WE and RE were suitably modified with PANI and PVA, respectively, in order to enhance the stability of the potentiometer battery. Subsequently, the HMNs sensor was implanted into the subject's forearm (Figure 7c) for evaluating its capability in monitoring bodily functions. Additionally, comprehensive *in vitro* characterization was conducted across a wide pH range spanning from pH 5 to pH 9, which aligns with the relevant index range for wound healing [71]. A remarkable performance was achieved, exhibiting a steep recurrence slope of  $-67.2 \pm 1.0 \text{ mV} \cdot \text{pH}^{-1}$  ( $N = 10$ ) (Figure 7d,e). The HMNs-based pH sensor demonstrates Nernstian response over an extensive linear range, making it suitable for real-time monitoring of interstitial fluid and wound healing-related pH levels.

Conversely, numerous researchers monitored pH levels by means of external sweat analysis [72–74]. Perspiration can be influenced by environmental conditions, such as temperature and humidity, as well as activity levels and chemical stimuli. While exercise is a reliable method to induce perspiration, meeting the demand for on-demand perspiration analysis in sedentary individuals poses challenges. Therefore, it is necessary to employ appropriate sweat stimulation methods that allow controlled sweat production for analytical applications. Ionophoresis (IP) is a commonly used chemical delivery process involving the application of an imperceptible local electric current to the skin, which stimulates sweat glands to produce sweat (e.g., pilocarpine) [75,76]. The highly integrated and flexible wearable sweat devices developed by Xu enable successful pH detection (Figure 8) [74]. The device is a non-invasive wearable sweat sensing patch comprising an electrochemical sensing system and a pilocarsin-based IP system, which was employed to stimulate sweat secretion. The electrochemical sensor utilized a tannin-silver-carbon nanotube-polyaniline (TA-Ag-CNT-PANI) hydrogel to modify the WE, and the hydrogel film exhibits excellent mechanical elasticity and structural stability. The sensor records the pH response ranging from 3.98 to 8.09, encompassing the entire pH range of sweat, and exhibits a sensitivity of  $-71.86 \text{ mV} \cdot \text{pH}^{-1}$ .



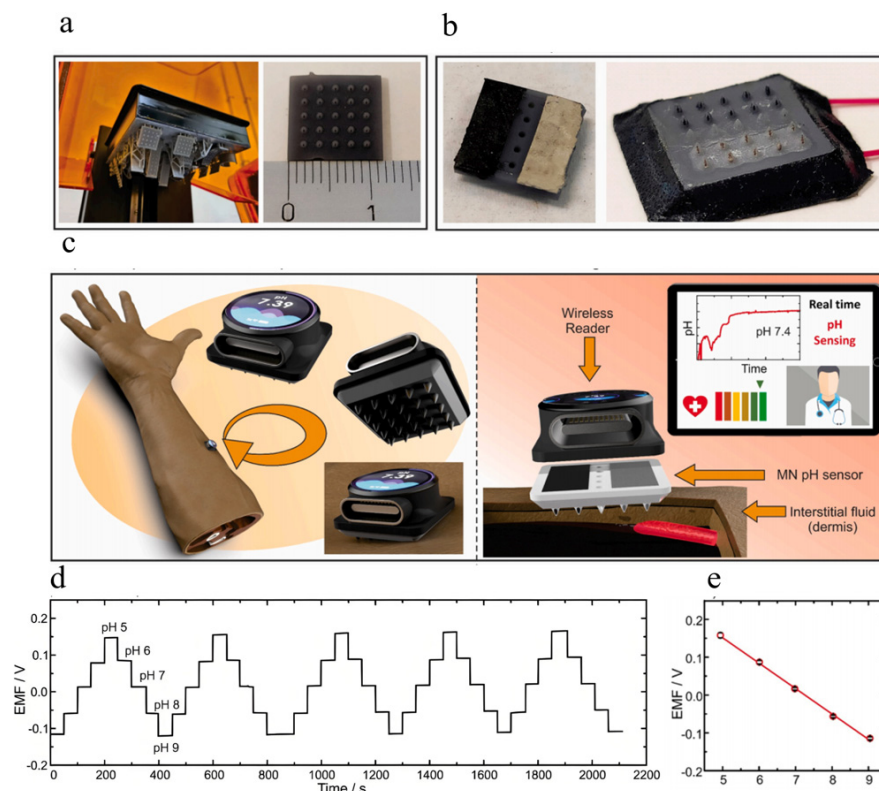


**Figure 7.** (a) Fabrication of the 3D-printed HMNs array. (b) The backside and frontside of HMNs-based potentiometric sensor. (c) Concept of the MN-based pH sensor pierced on the forearm of a subject for the transdermal monitoring of pH and full connectivity to healthcare service. (d) Reversibility test upon increasing and decreasing pH solutions from pH 9 to pH 5 during five cycles. (e) Corresponding calibration curves (N = 10). Reprinted with permission from ref. [70].

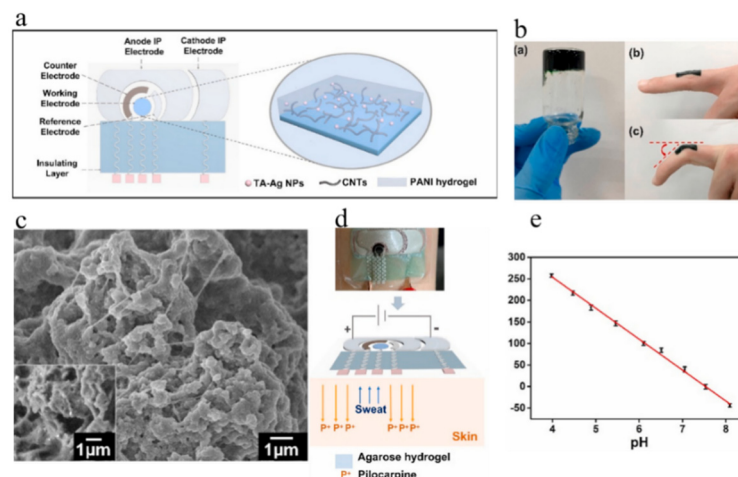


**Figure 8.** (a) Schematic illustration of the wearable sensor. (b) Photographs of TA-Ag-CNT-PANI hydrogel (inset a) and the hydrogels attached on the straight or bent fingers (inset b and c). (c) SEM of the TA-Ag-CNT-PANI hydrogel. (d) Schematic diagram of the operation, and the sweat was generated through the ionophoresis delivery of pilocarpine from the anode. (e) The linear calibration curve of the OCP response versus pH. Reprinted with permission from ref. [74].

### 2.1.2. Glucose

Diabetes is a metabolic disorder with multiple etiologies that manifests as hyperglycemia. The associated risks of diabetes include cardiovascular disease, retinopathy, nephropathy, neuropathy and other complications that can result in blindness, renal failure

and serious health consequences [77]. The prevalence of diabetes worldwide has witnessed a rapid surge in recent decades, and it is projected by the International Diabetes Federation that the global number of diabetes cases will escalate to 600 million by 2035 [78]. The presence of elevated blood glucose levels is a prominent characteristic in individuals diagnosed with diabetes, and when the blood glucose levels exceed 6.5 mM, it indicates the likelihood of diabetes [79,80]. Therefore, accurate and timely glucose detection is of paramount importance in safeguarding human lives. Electrochemical techniques have garnered significant attention for their cost-effectiveness, direct quantification capabilities, ease of miniaturization, and suitability for wearable devices compared to alternative methods such as colorimetry, optical coherence tomography, and near-infrared reflectance spectroscopy [81–85].

PANI is a promising material for modifying electrochemical sensor electrodes. Zhai developed a highly sensitive glucose sensor using PANI hydrogels [86]. The heterostructure and reaction mechanism of the glucose sensor, which is based on PtNPs/PANI, are depicted in Figure 9, showcasing the synergistic benefits derived from the integration of conductive polymer hydrogels (CPHs) and nanoparticles. The porous cross-linked structure of PANI facilitates the efficient immobilization of glucose oxidases and PtNPs, thereby enhancing the permeability for water-soluble molecules and effectively catalyzing glucose oxidation (Figure 9b). As shown in Figure 9c, the typical current–time response of the electrode at 0.56 V with continuous glucose addition. As the glucose concentration increases, the current increases immediately and quickly reaches a steady state. The average response time of the sensor is as short as 3 s (95% of steady-state current). Figure 9d shows the relationship between current and glucose concentration. In the concentration range of 0.01–8 mM, the steady-state current of the enzyme sensor was linearly correlated with the amount of glucose added to the buffer solution, and the correlation coefficient was 0.993. The calibrated linear portion calculated a sensitivity of up to  $96.1 \mu\text{A}\cdot\text{mM}^{-1}\cdot\text{cm}^{-2}$ , higher than previously reported values for sensor electrodes based on platinum and polyaniline composites, polypyrrole, or multi-walled carbon nanotubes (MWCNT).

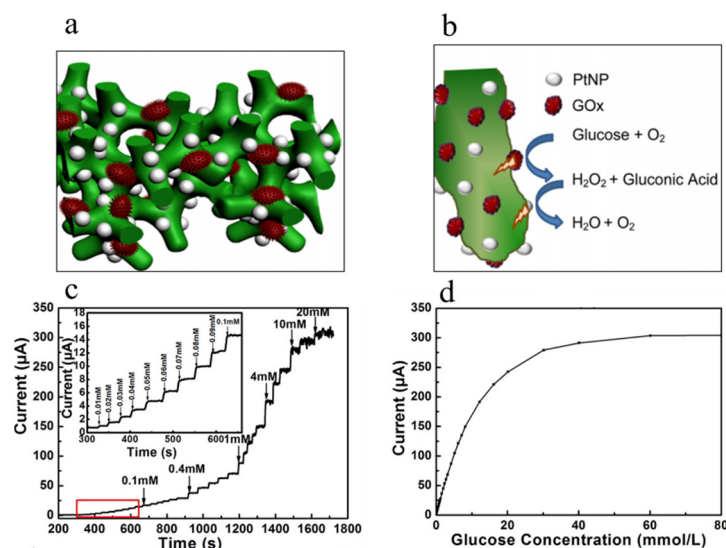


**Figure 9.** (a) The 3D heterostructural diagram depicts the integration of PtNPs/PANI hydrogels, wherein PANI hydrogels function as substrates for immobilizing GOx enzymes and facilitating uniform loading of PtNPs. (b) The reaction mechanism of glucose sensor based on PtNPs/PANI hydrogel electrode. (c) Amperometric response of the PtNPs/PANI hydrogel electrode after successive addition of glucose in 0.1 M PBS (pH = 5.6) at an applied potential of 0.56 V. Inset: the magnified part of the curve marked with red square. (d) The calibration curve for glucose concentrations from 0.001 to 80 mM. Reprinted with permission from ref. [86].

The integration of miniature sensors on a chip has led to the emergence of multiplexing as a prominent trend in biosensors, enabling simultaneous detection of multiple analytes. However, the precise deposition of electrode materials and selective enzymes on different microelectrode arrays remains a significant challenge for the mass production of multiplexed sensors. Li et al., introduced a three-indicator biosensor based on conductive PANI hydrogels, which was fabricated using an inkjet printing process [87]. The conductive PANI hydrogels were prepared using an all-solution method, enabling their deposition as the interface material through inkjet printing (Figure 10a–e). Subsequently, PtNPs and enzymes were precisely printed onto the designated working electrode. The PANI-based printed biosensor exhibits the capacity to simultaneously detect glucose, lactic acid, and triglycerides. Figure 10f–h records the detection mechanism of triglyceride, lactic acid, and glucose, as well as the instantaneous current–time relationship of the biosensor. It was found that the detection ranges of triglyceride, lactic acid and glucose were 0.1–6 mM, 0.08–5 mM, and 1–25 mM, respectively, and the detection limits were 0.07, 0.06, and 0.2 mM (S/N = 3). The linear range of these sensors can meet the requirements of human metabolic level sensing.

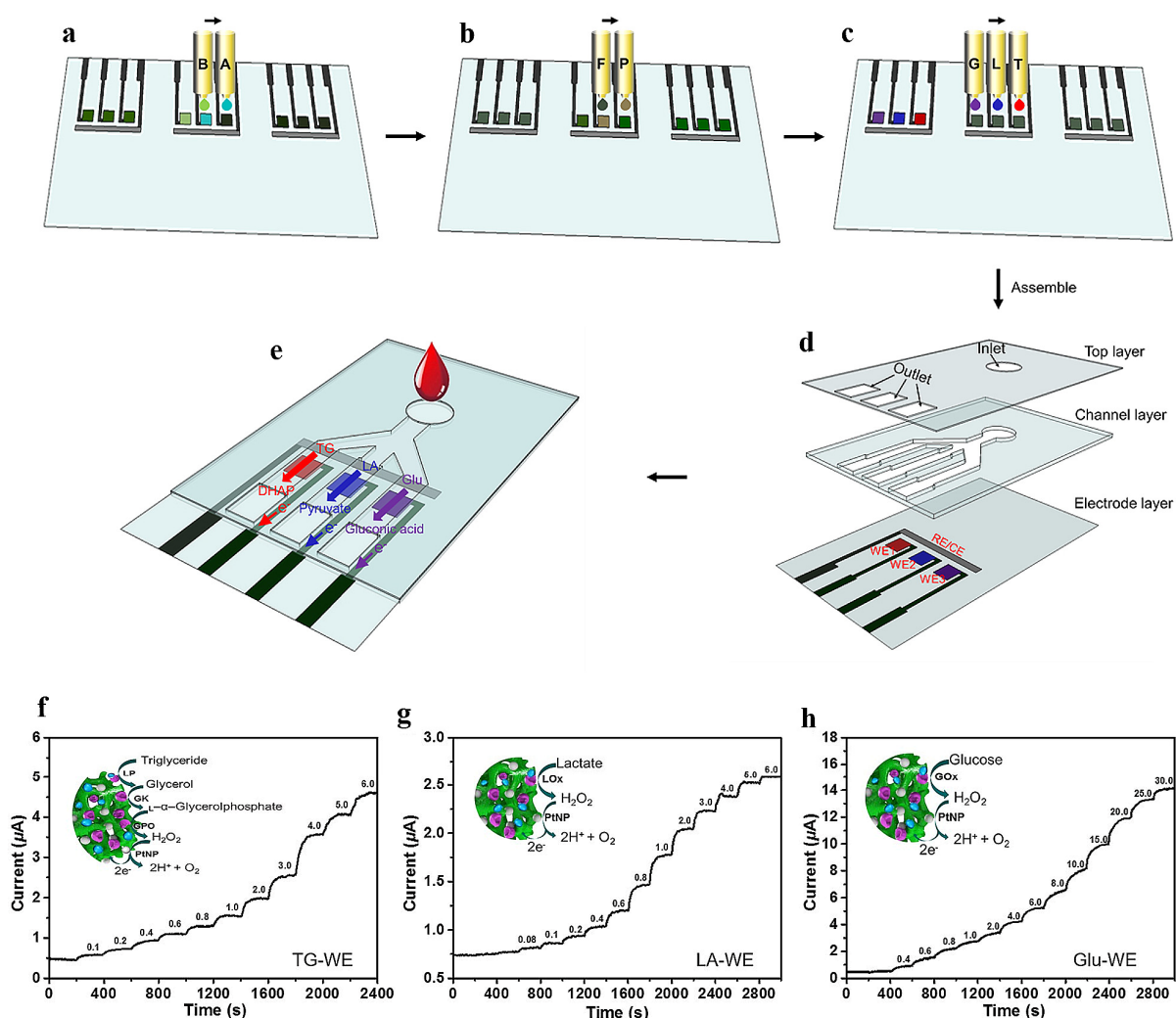


**Figure 10.** (a–e) Schematic diagram of design and manufacture of inkjet printing multi-channel biosensor based on conductive PANI hydrogels. (f–h) Instant current–time response curves of printed biosensors when metabolite solutions with different concentrations were pumped into the channel in an alternating manner. Reprinted with permission from ref. [87].

Pan et al., also developed CPs for glucose detection, utilizing a novel composite CPs electrode composed of MXene and conductive PEDOT/PSS hydrogel. They successfully

fabricated a non-invasive flexible electrochemical glucose sensor for continuous monitoring of human glucose levels through a simplified one-step synthesis method [88]. The PEDOT-PSS/MXene solution is mixed with ethylene glycol to enhance the polymer chain elongation and facilitate the formation of a homogeneous hydrogel solution. This approach effectively enhances the film-forming properties, flexibility, and stability of the material while mitigating issues related to powder accumulation and spalling. Moreover, this glucose biosensor demonstrated exceptional electrochemical performance in sweat, which exhibited a strong correlation with blood glucose concentration. Therefore, it is anticipated to further enhance the potential of non-invasive blood glucose monitoring.

The enzyme-free glucose electrochemical sensor is one of the sensors utilized for glucose detection. An enzyme-free glucose sensing microneedle was developed by combining PEDOT/PSS with Ag-Pt nanoparticles [89]. The low-cost hydrogel microneedle-continuous glucose meter method employed an expandable dopamine-hyaluronic acid hydrogel for the determination of glucose in dermal interstitial fluid. Platinum and silver nanoparticles were synthesized within a 3D porous hydrogel scaffold to enable non-enzymatic electrochemical sensing of glucose, while the incorporation of a highly aqueous dispersible conductive polymer enhanced the electrical properties of the hydrogel microneedle array, making it suitable for use as a working electrode in the sensor.

### 2.1.3. Cholesterol

Cholesterol is a vital structural component of both the plasma membrane and nerve cells [90]. The normal concentration of cholesterol in the blood can vary between 5.2 and 6.2 mM, depending on factors such as body weight, age, and sex. Hypercholesterolemia occurs when levels exceed 6.21 mM, which significantly increases the risk of myocardial infarction, atherosclerosis, high blood pressure, and coronary heart disease. Conversely, low cholesterol levels can lead to anemia and liver disease [91]. Therefore, accurately determining cholesterol is crucial for analyzing clinical diseases caused by its abnormality [92–94].

The conventional approach to cholesterol detection involves the utilization of an electrochemical cholesterol biosensor, which relies on the activity of cholesterol oxidase (ChOx). The selectivity of this sensor can be significantly enhanced through the incorporation of an enzyme electrode. Alagappan prepared a cholesterol biosensor based on AuNPs-f-MWCNTs-PPy-ChOx/GCE [95]. The biosensor was fabricated through a two-step process, involving the preparation of AuNPs-f-MWCNT via wet chemical method followed by electrical polymerization of pyrrole. PPy serves as a supportive matrix for immobilizing ChOx, while the presence of Au-f-MWCNT enhances conductivity. The PPy-based biosensor exhibited a linear response within the concentration range of 2–8 mM, demonstrating sensitivity and detection limits of  $10.12 \mu\text{A}\cdot\text{mM}^{-1}\cdot\text{cm}^{-2}$  and 0.1 mM, respectively. Li et al., developed and fabricated a biosensor platform based on CPHs [96]. The biosensor can be prepared using an all-solution process, utilizing phytic acid as both crosslinkers and dopants. The PANI hydrogel film can be formed within 3 min, while cholesterol esterase/cholesterol oxidase (ChEt/ChOx) was cross-linked in the PANI hydrogel matrix with the bifunction compound glutaraldehyde, enabling high-density and uniform deposition of the enzyme onto the three-dimensional nanostructure of polyaniline. Due to the unique characteristics of CPHs, such as their high permeability to biological substrates and rapid electron transfer, this biosensor exhibits excellent sensing performance with a wide linear range (0.3–9 mM), high sensitivity, low detection limit, and fast response time (approximately 3 s). Due to the easily scalable workability of CPs, the proposed CPs-based biosensor platform exhibits significant potential as a cost-effective sensor suite for medical monitoring, clinical diagnostics, and biomedical devices. A cholesterol biosensor without the need for enzymes can also be prepared by coating a screen-printed electrode with taurine (TA) modified PEDOT [97]. The sulfonic acid in TA forms electrostatic interactions with the polymerization main chain, exhibiting exceptional stability, high dispersion, and significant surface area adsorption of cholesterol through the induction matrix, thereby

enhancing its electrochemical performance. The results demonstrate that the sensor exhibits an extremely low detection limit of 0.95  $\mu\text{M}$  ( $S/N = 3$ ), enabling rapid detection of low concentrations of cholesterol in various bodily fluids.

#### 2.1.4. DNA and RNA

Although society is making continuous progress, it also faces numerous challenges stemming from these advancements, such as the prevalence of life-threatening diseases that include cancer, genetic disorders, and infectious ailments. The identification and diagnosis of these sicknesses hold paramount importance, thus necessitating the utilization of electrochemical biosensors as potent bioanalytical tools, particularly for nucleic acid detection. Electrochemical DNA (E-DNA) sensors are favored by researchers for their fast response time, accurate measurement and stability, and seamless integration with electronic devices [98–102].

The application of the E-DNA sensor relies on the process of DNA hybridization [103]. Kiransan et al., developed polymer-supported graphene-based materials utilizing DNA hybridization for electrochemical determination [104]. The first step involved transforming a polymer dispersion of graphene oxide (GO) and PEDOT/PSS with varying compositions into a hydrogel through hydrothermal treatment. Subsequently, a 3D flexible composite sponge material consisting of PEDOT/PSS and reduced graphene oxide (RGO) was prepared using the freeze-drying technique (Figure 11a). The structural and morphological characterization results revealed that the PEDOT/PSS polymer formed a mesh-like structure, effectively covering the graphene layer, thereby providing support and enhancing the mechanical strength and electrochemical performance of the 3D material through a reduction in pore size (Figure 11b). The PEDOT-PSS/RGO composite sponge exhibits a significantly high electrical conductivity of  $158 \text{ S}\cdot\text{cm}^{-1}$ , making it suitable for use as an electrode. Additionally, its durability is enhanced by a remarkable factor of 700. The MB-ssDNA probes, labeled with single-stranded DNA (ssDNA) and methylene blue (MB), were immobilized onto a PEDOT-PSS/RGO composite sponge. Subsequently, electrochemical assays were conducted under optimized conditions (Figure 11c). The detection limit of the sensor can be reduced to 17 fM, and the linear range spans from  $5 \times 10^{-11}$  to  $2 \times 10^{-3}$  mM, rendering it suitable for the detection of hybrid DNA.

The PANI/PA hydrogels with a mesoporous structure were synthesized by Yang using a one-step electrochemical method and have been utilized for the detection of microRNA [105]. The biosensor was developed by immobilizing the DNA probe onto the PANI/PA interface and utilizing the REDOX current of PANI as the sensing signal for detecting DNA/RNA hybridization reaction (Figure 12). Due to the characteristic properties of PANI/PA hydrogels, this biosensor exhibits a wide linear range ( $1 \times 10^{-12}$ – $1 \times 10^{-9}$  mM), a low detection limit (0.34 fM), and efficient detection capability for microRNA mismatch. Importantly, PANI/PA hydrogels not only offer a plethora of active sites for DNA immobilization but also generate inherent electrochemical signals through the reduction and oxidation reactions in PANI, eliminating the need for additional REDOX probes.

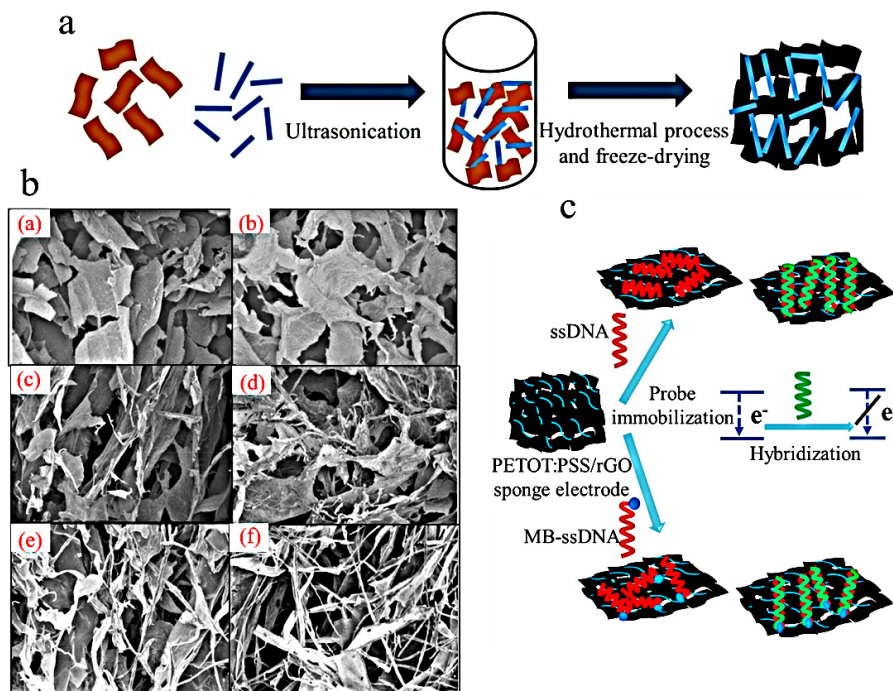


**Figure 11.** (a) Schematic illustration of the preparation of PEDOT–PSS/RGO composite sponge material. (b) SEM images of RGO (a), PEDOT–PSS-2/RGO (b), PEDOT–PSS-4/RGO (c), PEDOT–PSS-6/RGO (d), PEDOT–PSS-8/RGO (e), and PEDOT–PSS-10/RGO (f). (c) Schematic representation of the immobilization and hybridization of ssDNA and MB-ssDNA probes onto the PEDOT–PSS/RGO composite sponge material. Reprinted with permission from ref. [104].

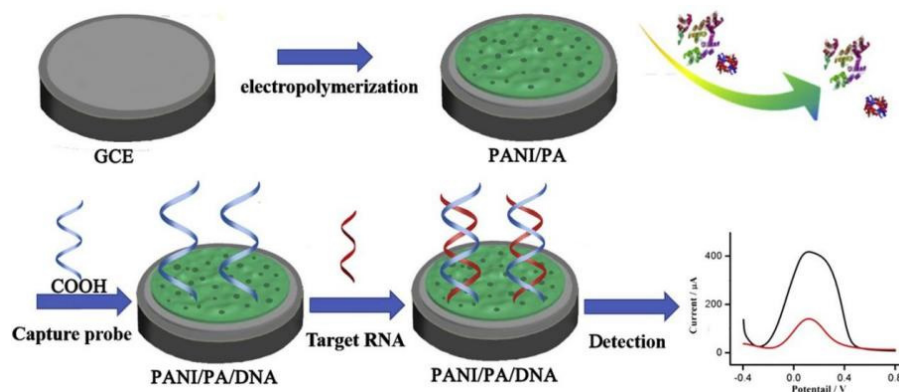


**Figure 12.** The structure of PANI/PA interface and its application for miRNA sensor. Reprinted with permission from ref. [105].

### 2.1.5. Other Substances

The range of biomolecules is extensive, encompassing tryptophan [106,107], dopamine [108,109], and various others in addition to those previously mentioned. Among the crucial indicators that facilitate various physiological processes, tryptophan plays a vital role in protein synthesis and serves as a significant precursor to serotonin. Being an indispensable amino acid, tryptophan exerts profound influence on human health [110,111]. Xu’s team incorporated PEDOT/PSS into a zwitterionic PSBMA (poly-sulfobetaine methacrylate) network to fabricate an innovative semi-interpenetrating hydrogel [112]. This versatile hydrogel lays the foundation for the development of a stain-resistant wearable molecularly imprinted sensor capable of sensitive and robust detection of tryptophan in complex sweat. Dopamine modulates motor, affective, cognitive, and endocrine functions within the central nervous system, while also playing a role in the regulation of vasoconstriction. Rishabh Bansal’s team prepared the

fabrication of a flexible sensor based on a hybrid nanocomposite of self-supporting polypyrrole electrode modified copper nanoparticles (PPy-Cu) for the electrochemical detection of dopamine [113]. The sensing capability of the self-standing PPy-Cu electrode was evaluated by chronoamperometry and optimized for different copper deposition times. PPy-Cu 120 has good dopamine detection performance. The lower limit of detection was 1.19  $\mu\text{M}$ , and the linear range was  $2.5 \times 10^{-3}$ – $2.5 \times 10^{-1}$  mM. In addition, this self-standing sensor is entirely composed of polypyrrole (a biocompatible polymer) and copper nanoparticles, making it sustainable and environmentally friendly. These encouraging results pave the way for the development of the next generation of flexible sensors that detect neurotransmitters and environment-related analytes.

## 2.2. Cancer Markers

The accurate detection of disease biomarkers in human body fluids, such as blood, urine, and saliva, with high sensitivity and specificity is crucial for early disease diagnosis and effective treatment [114–116]. The immunochemical methods based on antigen–antibody interactions have been widely adopted in daily clinical practice as the preferred approach for sensitive and reliable detection of protein-based cancer biomarkers in body fluids [117–119]. Over the years, various immunochemical methods have been developed, with electrochemical immune sensors being the preferred choice among scientists. However, the limited conductivity, small surface area, and poor anti-interference capabilities of general electrochemical immune sensors have hindered their development. The issue was addressed by scientists through the introduction of CPs, which fix antibodies within a network structure of these polymers using binders. This approach significantly increases the contact area and accelerates electron transmission while enhancing anti-interference ability [120,121].

Aydin developed an immunosensor utilizing gold nanoparticles/amino-functionalized thiophene polymer (AuNPs/P(ThiAmn)) for impedance-based detection of GM2 activating protein (GM2A) [122]. The AuNPs/P(ThiAmn) multilayer films were fabricated using electrochemical synthesis technology, thereby yielding conductive multilayer films suitable for biosensor applications. Due to the increased surface area and enhanced electron transfer properties of AuNPs and conjugated polymers, numerous anti-GM2A antibodies were attached to the amino group of P(ThiAmn) polymers. As a result, the modified electrode surface was prepared for the selective analysis of GM2A. Even in the presence of other interfering biomolecules, the proposed biosensor exhibits exceptional analytical detection performance with high sensitivity and specificity towards GM2A. Under optimal conditions, electrochemical impedance spectroscopy (EIS) enables determination of GM2A within a linear concentration range of 0.0185–111  $\text{pg}\cdot\text{mL}^{-1}$ , achieving a limit of detection as low as 5.8  $\text{fg}\cdot\text{mL}^{-1}$ . Similarly, Zhao et al., utilized AuNPs embedded within multiple 3D layers in various CPs substrates, such as poly (thiophen-3-acetic acid), poly (pyrrolio-2-carboxylic acid), and poly (pyrrolio-3-carboxylic acid), exploiting their extensive surface area and superior conductivity as transducers [123]. The identification of Amyloid- $\beta$  oligomers ( $\text{A}\beta\text{O}$ ), which are believed to be responsible for the neurotoxic effects associated with Alzheimer's disease, was specifically accomplished by utilizing cellular prion protein (PrPC) as a biometric component. The PrPC/AuNPs embedded PPy-3-COOH matrix exhibits enhanced sensitivity and an extended detection range ( $10^{-15}$ – $10^{-9}$  mM). Additionally, a high-performance sensor based on a double-template molecularly imprinted polymer has been successfully utilized for the specific detection of lung cancer biomarkers carcinoembryonic antigen (CEA) and alpha-fetoprotein (AFP) [124]. The impedance method was employed to detect the rebinding of template antigens, wherein an increase in charge transfer resistance was observed with escalating concentrations of CEA and AFP. The linear dynamic ranges for CEA and AFP were 5– $10^4$  and 10– $10^4$   $\text{pg}\cdot\text{mL}^{-1}$ , respectively, while the detection limits stood at 1.6 and 3.3  $\text{pg}\cdot\text{mL}^{-1}$ .

Kilic has developed a novel CPs material called zwitterionic polypyrrole (ZiPPy), which offers optimal surface conditions for biosensing electrodes (Figure 13) [125]. ZiPPy

possesses two distinct advantages: the zwitterion functionality effectively hydrates the electrode surface and impedes non-specific binding of hydrophobic proteins. Compared to bare and PPy-modified electrodes, the ZiPPy-modified electrode exhibits lower electrochemical impedance and reduced non-specific protein adsorption (low dirt). Furthermore, in a one-step electropolymerization process, affinity ligands for target biomarkers can be immobilized with ZiPPy. Specifically, a ZiPPy-modified electrode was designed for the detection of severe acute respiratory syndrome Coronavirus 2 (SARS-CoV-2), achieving a LOD as low as  $5 \times 10^{-4}$  pg·mL<sup>-1</sup> in human saliva without the need for sample purification or secondary labeling.

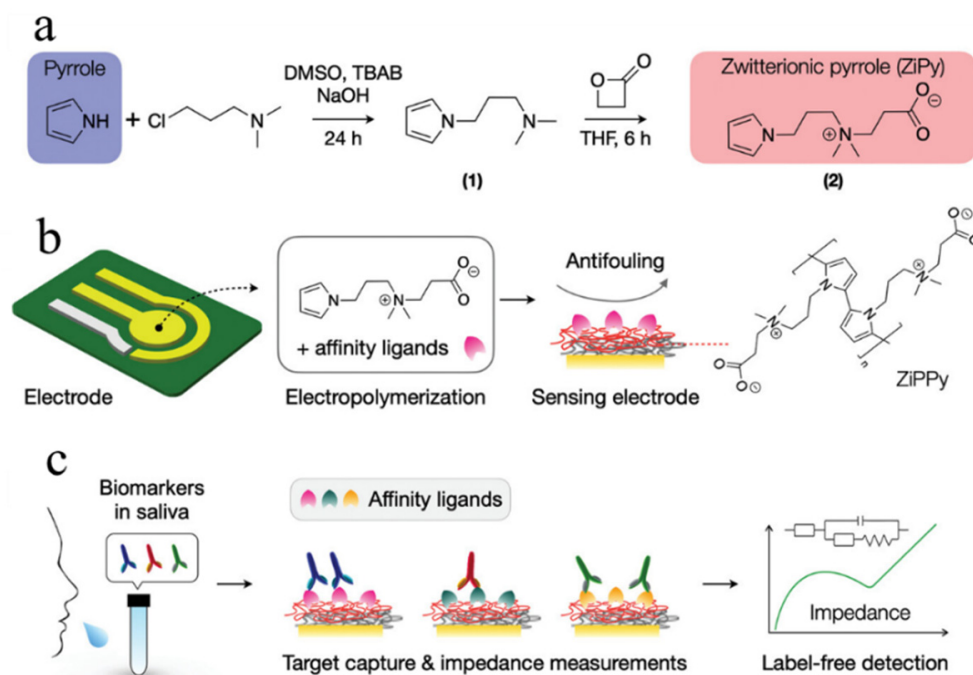


**Figure 13.** (a) Pyrrole is reacted with 3-dimethylaminopropylchloride hydrochloride to produce N, N-dimethyl-3-(1H-pyrrol-1-yl) propan-1-amine and then converted to ZiPy. (b) A mixture of affinity ligands and ZiPy monomers is drop-cast on electrodes. (c) Antibodies (target biomarker) present in saliva are captured by different antigens immobilized on ZiPPy-modified electrodes. Reprinted with permission from ref. [125].

### 2.3. Drug Screening and Delivery

The role of CPs-based sensors in drug screening and delivery is to monitor drug release in real time, assess drug activity and efficacy, and evaluate the biocompatibility of drug carrier materials to support precision therapy.

Bipolar disorder is a chronic psychiatric condition that imposes significant social and economic burdens, characterized by pronounced mood fluctuations in affected individuals [126,127]. Valproic acid is the first-line pharmacological treatment for stabilizing daily mood in patients with bipolar disorder [128]. However, elevated levels of valproic acid in the bloodstream can lead to severe adverse reactions, necessitating regular monitoring of blood valproic acid concentrations in patients [129]. Yuan et al., developed an innovative electrochemical sensor for the selective and facile detection of valproate, utilizing a molecularly imprinted polymer film prepared via one-step electro-polymerization [130]. The binding of the target molecule to the custom bionic PPy membrane of valproic acid obstructs the cavity within the membrane and induces alterations in its electrical properties, which can be detected through differential pulse voltammetry (DPV) as a reduction in peak current. The peak current changes exhibited a strong logarithmic response to the concentration of valproate. Similarly, tramadol (TRA) is a weak opioid analgesic utilized for the management of mild to moderately severe pain [131]. However, excessive use of TRA has



been frequently associated with adverse effects such as vomiting, depression, tachycardia, convulsions, morbidity, and mortality [132]. Diouf developed an electrochemical sensor based on a molecularly imprinted conductive polymers (MICP) for the quantitative and non-invasive detection of TRA [133]. The MICP-based sensor was fabricated by employing self-assembly techniques to deposit a layer of PANI coated with silver nanoparticles (AgNPs) onto a screen-printed gold electrode (Au-SPE), followed by polymerization of 2-aminothiophene in the presence of TRA. Under optimized conditions, the response of this sensor is directly proportional to the concentration of TRA within the range from  $1 \times 10^4$  to  $1 \times 10^8$   $\text{pg}\cdot\text{mL}^{-1}$ .

An updated comparative list of different CPs applications in biomedicine is presented in Table 1.

**Table 1.** The main electrochemical sensors based on CPs and their parameter analysis, the application of electrochemical technology and its application in biomedical detection are introduced.

CPs	Analyte	LOD (mM)	Linear Range(mM)	Application	Ref.
PANI	PH	0.0014	$10^{-5}$ –0.1	Biomolecular detection	[70]
PANI	pH	0.0016	$8 \times 10^{-6}$ –0.1	Biomolecular detection	[74]
PANI	Glucose	0.0007	0.01–8	Biomolecular detection	[86]
PANI	Glucose	0.2	1–25	Biomolecular detection	[87]
PEDOT/PSS	Glucose	0.0019	$10^{-3}$ –0.094	Biomolecular detection	[88]
PEDOT/PSS	Glucose	0.0009	0.094–1.294	Biomolecular detection	[89]
PPy	Cholesterol	0.1	0.0002–0.5	Biomolecular detection	[95]
PANI	Cholesterol	0.00095	2–8	Biomolecular detection	[96]
PEDOT/PSS	DNA	$1.7 \times 10^{-11}$	0.003–1	Biomolecular detection	[104]
PANI	microRNA	$3.4 \times 10^{-13}$	$5 \times 10^{-11}$ – $2 \times 10^{-3}$	Biomolecular detection	[105]
PEDOT/PSS	tryptophan	0.00067	$1 \times 10^{-12}$ – $1 \times 10^{-9}$	Biomolecular detection	[112]
PPy	Dopamine	0.00119	0.002–0.1	Biomolecular detection	[113]
PTH	GM2A	$2.13 \times 10^{-11}$	$2.5 \times 10^{-3}$ – $2.5 \times 10^{-1}$	Cancer makers	[122]
PPy	A $\beta$ O	10–15	$6.79 \times 10^{-11}$ – $4.07 \times 10^{-7}$	Cancer makers	[123]
PPy	CEA, AFP	$5.87 \times 10^{-12}$ , $1.21 \times 10^{-11}$	$10^{-15}$ – $10^{-3}$	Cancer makers	[124]
PPy	SARS-CoV-2	$1.84 \times 10^{-4}$	$1.83 \times 10^{-11}$ – $3.67 \times 10^{-8}$ , $3.67 \times 10^{-11}$ – $3.67 \times 10^{-8}$	Cancer makers	[125]
PPy	Valprate	0.01748	$5.5 \times 10^{-12}$ – $3.67 \times 10^{-7}$	Drug screening and delivery	[130]
PANI	TRA	0.0346	$1.84 \times 10^{-14}$ – $2.75 \times 10^{-13}$	Drug screening and delivery	[133]

### 3. Environmental Applications

Electrochemical sensors based on CPs have been extensively utilized in environmental monitoring, encompassing the determination of nitrate nitrogen, heavy metals, antibiotics, and pesticides in soil and water environments. Additionally, they have also been employed for the detection of toxic gases.

#### 3.1. Nitrate Nitrogen

The expansion of industrialization and excessive fertilizer use in agriculture contribute to the escalation of nitrate pollution in water and soil [106,134]. Overuse of nitrate leads to increased algae growth, contamination of groundwater and surface water, and ecological damage. Moreover, excessive intake of nitrate by humans can cause various complications [135]. Bacterial enzymes convert nitrate to nitrite in the human digestive system, disrupting hemoglobin's oxygen transportation function and causing symptoms of hypoxia [136,137]. Additionally, it reacts with amines in the gastrointestinal tract to produce carcinogens [138]. Nitrate presence can also lead to other health issues such as headaches, nausea, and vomiting. Therefore, developing an accurate and efficient method for detecting nitrate is crucial.

Both Zhang's and Motaghedifard's teams have developed all-solid ion selective electrode (ASS-ISE) that incorporate CPs and other nanoparticles for the detection of nitrate

ion [139,140]. While the main difference lies in the selection of modified CPs at the electrode interface. The sensor developed by Zhang's group utilizes a molecularly imprinted PPy membrane and exhibits a linear range of  $5.25 \times 10^{-2}$ – $1 \times 10^2$  mM, with a response slope of  $-50.4 \text{ mV} \cdot \text{dec}^{-1}$  [139]. The molecularly imprinted PPy membrane significantly improves the limitations of the PVC sensitive membrane, while incorporating AuNPs to enhance electrical conductivity and promote stronger bonding properties. Motaghedifard's research group developed a hybrid nanocomposite of Au-modified MWCNT/Cu/PANI for the detection of nitrate ions [141]. This sensor utilizes precious metal bimetallic nanoparticles (gold and copper) to catalyze the reduction of nitrates in polymer carbon modifiers, achieving a remarkable detection limit of  $0.09 \mu\text{M}$ . The electrode has been successfully employed for the determination of nitrate ions in both industrial wastewater and aqueduct water from a barium chromate production line.

The continuous measurement of nitrate nitrogen holds significant potential applications in the fields of plant biology, plant breeding, environmental science, and agricultural production. In contrast to the aforementioned preparation of ASS-ISEs, Ali reported a novel ASS-ISE for real-time continuous monitoring of soil nitrate levels [142]. The patterned gold WE of this sensor was modified with poly(3-octylthiophene) and molybdenum disulfide (POT-MoS<sub>2</sub>). The POT-MoS<sub>2</sub> layer acts as an ion-to-electron transduction layer, possessing high hydrophobicity and REDOX properties. This layer significantly enhances conductivity and anion exchange while minimizing the formation of a thin water layer at the interface between the Au electrode and the ion-selective membrane (ISM). Consequently, this sensor exhibits exceptional performance in terms of selectivity, sensitivity, and long-term stability even when exposed to significant concentrations of other anions. Vapor phase polymerization (VPP) is a common technique for directly polymerizing gaseous monomers into polymers under gas phase conditions [143]. In the VPP process, monomer gases undergo a series of chemical reactions in the gas phase to form a polymer film or coating [143]. By employing VPP technology, Kohler's group prepared a real-time sensor based on PEDOT for the detection of nitrate ions through monitoring changes in electrical properties [144]. The sensitivity of the sensor to nitrates is influenced by various polymerization parameters such as temperature, pressure, and time. Under optimized conditions, the sensor exhibits a resistance response of 41.79% to a nitrate solution concentration of 1000 ppm. Furthermore, it has the capability to detect nitrate concentrations ranging from 1 ppm to 1000 ppm. The proposed sensor demonstrates significant potential for the real-time monitoring of excessive nitrate ions in aqueous solutions.

### 3.2. Heavy Metal Ions

The presence of heavy metal ions (HMIs) in water, soil, and other natural environments is a significant environmental concern. These pollutants originate from various sources such as nature, industrial discharges, agricultural activities, sewage treatment plants, and drinking water pipes. Due to their high toxicity and non-degradability, HMIs pose serious threats to the ecological environment as well as public and human health. The toxic metal ions, such as cadmium ( $\text{Cd}^{2+}$ ), lead ( $\text{Pb}^{2+}$ ), mercury ( $\text{Hg}^{2+}$ ), cobalt ( $\text{Co}^{2+}$ ) and others, exhibit high mobility in aquatic environments and have a propensity for bioaccumulation along the food chain, thereby posing a potential risk to human health even at low concentrations [10,145]. The detrimental effects of HMIs on the human body are mediated through various mechanisms, including induction of oxidative stress, DNA damage, impairment of protein function, initiation of cell apoptosis, and promotion of inflammatory reactions [146].

Xiao et al., designed and prepared a 3D high-porosity CPHs-based sensor, which successfully enabled the detection of  $\text{Cd}^{2+}$ ,  $\text{Cu}^{2+}$ ,  $\text{Pb}^{2+}$  and  $\text{Hg}^{2+}$  [147]. The synthesis of a g-C<sub>3</sub>N<sub>4</sub>-P(ANI-Py)-PAAM polymer hydrogel involved the crosslinking of aniline pyrrole copolymer with acrylamide, phytic acid as both dopant and crosslinking agent, followed by integration with g-C<sub>3</sub>N<sub>4</sub> (Figure 14). The 3D mesh high-porosity hydrogels not only exhibit excellent electrical conductivity, but also offer a substantial surface area for augmenting

the population of immobilized ions [148]. The LOD for  $\text{Cd}^{2+}$ ,  $\text{Cu}^{2+}$ ,  $\text{Pb}^{2+}$  and  $\text{Hg}^{2+}$  by this sensor were determined to be  $2.608 \times 10^{-5}$  mM,  $5.323 \times 10^{-5}$  mM,  $1.484 \times 10^{-5}$  mM and  $6.835 \times 10^{-5}$  mM, respectively, making it suitable for trace analysis. In addition, the sensor demonstrates exceptional accuracy in lake water quality assessments. The preparation and implementation of hydrogels in electrochemical sensors offer a viable approach for the electrochemical capture and detection of diverse hazardous materials in solution, thereby presenting significant prospects for commercial applications. The group led by Kulkarni has also developed a sensor utilizing PPy to detect HMIs, effectively combining the exceptional properties of graphene nanoribbons (GNR) with conductive PPy [149]. GNR was synthesized via the MWCNT decompression method, while GNR/PPy was synthesized through in situ polymerization. The material comprises multiple layers of carbon and nitrogen that facilitate binding to  $\text{Pb}^{2+}$ . The modified electrochemical sensor exhibited significantly enhanced peak current intensity for the rapid detection of  $\text{Pb}^{2+}$ , achieving a remarkable detection limit of 0.03 nM. Moreover, the electrode demonstrated exceptional selectivity towards  $\text{Pb}^{2+}$ , even in the presence of  $\text{Cu}^{2+}$ ,  $\text{Zn}^{2+}$ , and  $\text{Hg}^{2+}$ .

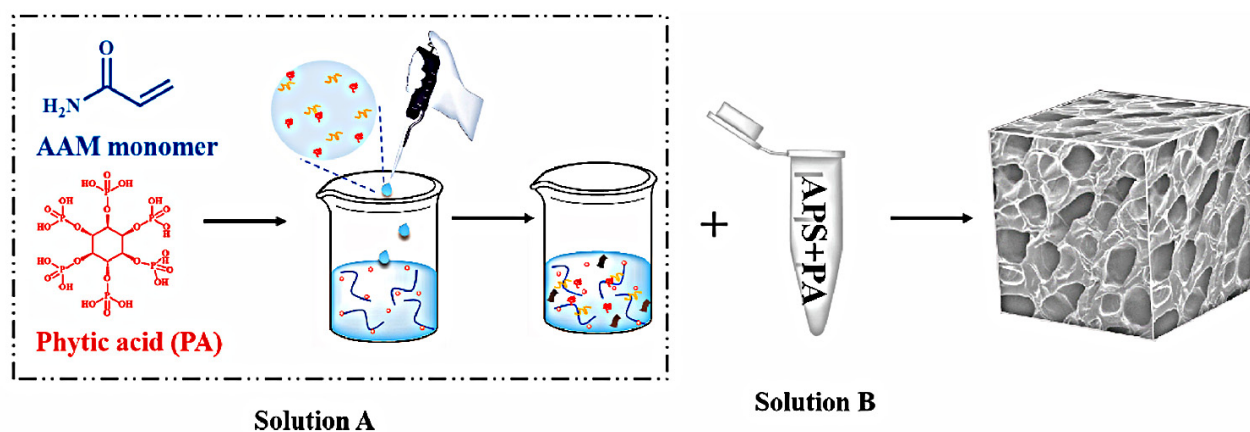


**Figure 14.** Schematic diagram of  $\text{g-C}_3\text{N}_4\text{-P(ANI-Py)-PAAM}$  polymer hydrogel synthesis. Reprinted with permission from ref. [147].

The utilization of PANI as an interface modification material for HMIs detection is also investigated [150]. The composites of polyaniline-benzothiazole [(3,5-bis(benzo[d]thiazol-2-yl)-[1,1-biphenyl]-4-ol)] (PANI-BEN) were synthesized for the detection of  $\text{Hg}^{2+}$  and  $\text{Pb}^{2+}$ , achieving detection limits of 1pM and 4.6pM, respectively [151]. Some researchers have investigated the combination of metal–organic frameworks (MOFs) and PANI [152]. PANI was synthesized in both conductive (emerald salt, ES) and non-conductive forms (emerald base, EB), with six different mass ratios of MOF-5 and PANI used to produce the conjugated polymer. The electrochemical response of all composites towards the presence of  $\text{Cd}^{2+}$  and  $\text{Pb}^{2+}$  is consistently observed. Among them, the MOF/EB-1 composite with 71.0 wt.% MOF-5 exhibits the highest oxidation current when both HMIs are detected individually or simultaneously. The current density recorded by MOF/EB-1 is also higher than that of its individual components, indicating a synergistic effect wherein MOF-5 offers a substantial surface area for the adsorption of  $\text{Cd}^{2+}$  and  $\text{Pb}^{2+}$ , while PANI facilitates an electron transfer network during the subsequent metal oxidation.

Furthermore, a novel composite consisting of a mercaptan (-SH) grafted polymer (3,4-propenedioxythiophene)/porous silicon sphere (PProDOT( $\text{MeSH}$ )<sub>2</sub>@Si) has been employed for the electrochemical detection of  $\text{Cd}^{2+}$ ,  $\text{Pb}^{2+}$  and  $\text{Hg}^{2+}$  (Figure 15) [153]. The PProDOT( $\text{MeSH}$ )<sub>2</sub>@Si composite was synthesized via chemical oxidation polymerization, and the detection of  $\text{Cd}^{2+}$ ,  $\text{Pb}^{2+}$  and  $\text{Hg}^{2+}$  was performed using differential pulse voltammetry (DPV). The results demonstrated that the incorporation of two sulfhydryl chains into the monomer unit enhances the electrochemical sensitivity of PProDOT( $\text{MeSH}$ )<sub>2</sub>, which can be attributed to the interaction between sulfhydryl (-SH) groups and heavy metal

ions. Moreover, the integration of PProDOT(MeSH)<sub>2</sub> with porous Si sphere significantly improves the electrocatalytic efficiency of the electrode material.

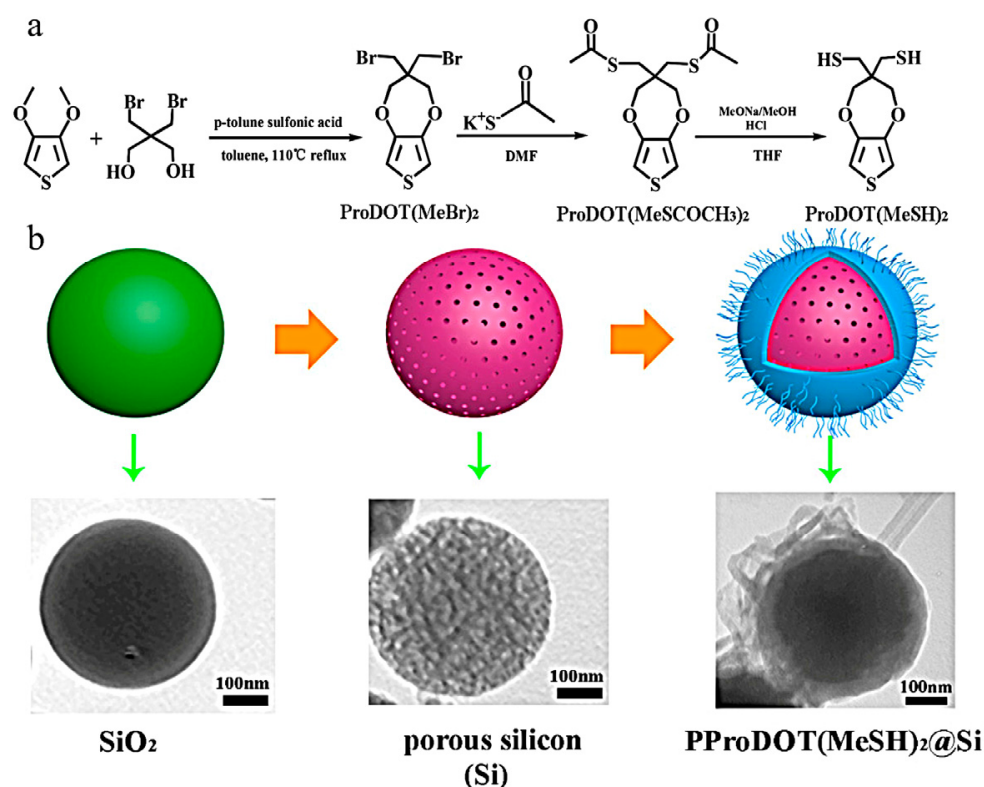


**Figure 15.** (a) The synthesis route of double-thiol linked (3,4-proplenedioxythiophene) ProDOT(MeSH)<sub>2</sub> monomer. (b) PProDOT(MeSH)<sub>2</sub>@Si synthesis route. Reprinted with permission from ref. [153].

### 3.3. Antibiotics

Concern over the hazardous accumulation of antibiotics in food and water resources has significantly increased in the past decade. The excessive use and improper disposal of antibiotics, as well as the discharge of animal and human waste, aquaculture practices, hospital and industrial waste, along with inefficient removal during conventional water treatment processes contribute to the build-up of antibiotics in both food and the environment. Consequently, antibiotics have been identified as an emerging environmental pollutant in recent years [154–156].

Cefixime (CEF, a semi-synthetic antibiotic, third-generation cephalosporin) exhibits bactericidal properties by inhibiting bacterial cell wall formation, growth, and proliferation, ultimately leading to bacterial death [157]. A novel electrochemical sensor was developed by incorporating expanded graphene oxide and gold nanowires, followed by the electrical polymerization of PANI MIPs on the electrode surface [158]. This sensor demonstrates linear response within a concentration range of  $2 \times 10^{-5}$ – $9.5 \times 10^{-4}$  mM with a detection limit of 7.1 nM.

Sulfonamides (SAs) are a class of broad-spectrum synthetic antibacterial and anti-inflammatory antibiotics, including sulfamethizole, sulfadiazine, and sulfisoxazole. Due to their high efficacy and cost-effectiveness, SAs have been extensively utilized for the prevention and control of human and animal infections as well as for promoting animal husbandry growth [159]. Kong's group demonstrated a reusable and label-free electrochemical sensor utilizing an electropolymeric MIP film as an identification layer for rapid and sensitive detection of sulfamethazole [155]. In order to achieve effective identification, computational simulation and subsequent experimental evaluation were conducted for monomer screening of four 3-substituted thiophenes, ultimately selecting 3-thiophene ethanol. The synthesis of MIPs is rapid and environmentally friendly, allowing for in situ

manufacturing on the sensor surface. Under optimized experimental conditions, the sensor exhibits a good linear relationship within the range of  $1 \times 10^{-6}$ – $1 \times 10^{-2}$  mM, with a detection limit as low as 0.18 nM.

Oxacillin (OXC) is a penicillin-based antibiotic commonly employed for the treatment of infections caused by susceptible strains, including those affecting the respiratory tract, skin, soft tissues, and other infection symptoms. The mechanism of action of oxacillin involves inhibiting bacterial cell wall synthesis, ultimately leading to bacterial death [160]. The screen-printed carbon electrode (SPCE) was utilized to fabricate an oxacillin sensor. The SPCE underwent modification with nano-gold and graphene oxide, followed by electropolymerization of aniline in the presence of graphene oxide [156]. Under a typical peak potential of 0.82 mV (relative to Ag/AgCl), the response exhibited a linear range spanning from  $7 \times 10^{-7}$  to  $5.75 \times 10^{-4}$  mM. The sensitivity was determined as  $9.76 \times 10^4 \mu\text{A} \cdot \text{mM}^{-1} \cdot \text{cm}^{-2}$ , while the detection limit stood at  $2 \times 10^{-7}$  mM. In the case of a concentration of OXC at  $2 \times 10^{-4}$  M, the relative repeatability for six repeated experiments was found to be 2.6%.

Dimetronidazole (DMZ), a derivative of nitroimidazole, is a veterinary drug used as an antibiotic to treat bacterial or protozoan infections in poultry. The electrochemical detection of DMZ was conducted using SPCE modified with PANI-Cu@BSA/RGO nanocomposites [161]. The PANI-Cu@BSA electrocatalyst was synthesized through one-step biomimetic mineralization polymerization, utilizing bovine serum albumin (BSA) as a stabilizer. And the PANI-Cu@BSA/reduced graphene oxide (RGO) nanocomposites were prepared through ultrasonic coating, exhibiting exceptional water dispersibility, high electrical conductivity, and nano-sized particles. The increase in current intensity primarily stems from the enhanced rapid electron transfer between the electrode and the analyte, facilitated by the combination of PANI-Cu@BSA with RGO. This synergistic effect leads to an exceptional electrical conductivity and active surface area at the analyte–electrode junction.

### 3.4. Pesticide

Pesticide residues can pose various risks to human health, primarily through the long-term consumption of food containing such residues, which may result in chronic poisoning and adversely affect the nervous system, endocrine system, immune system, among others. This can lead to chronic diseases like cancer and nervous system dysfunction. Children and pregnant women are particularly vulnerable to pesticide residues as their growth and development can be negatively impacted by prolonged exposure, increasing the risk of adverse effects and disease. Furthermore, pesticide residues not only harm human health but also contribute to soil and water pollution while disrupting ecological balance [162].

To tackle this problem, researchers have devised electrochemical sensors utilizing CPs to detect pesticide residues. The electrochemical sensor developed by Anirudhan utilized a combination of MWCNT and CPs to effectively detect chlorpyrifos (CPF) in vegetable sample solutions [163]. The copolymerization of 3-thiophenic acid and 3,4-ethylenedioxythiophene was conducted on the surface of MWCNTs, followed by drop-casting onto the electrode surface for highly sensitive detection of CPF. Under optimal conditions, the sensor has an extremely low detection limit of 0.004 nM. The detection of glyphosate (Gly) was accomplished by Ding through the utilization of molecularly imprinted PPy nanotubes, which were fabricated by imprinting Gly binding sites onto the surface of PPy nanotubes [164]. The modified SPCE electrode exhibited excellent conductivity and rapid adsorption rate, as well as enhanced affinity and specificity towards Gly. The portability of this sensor makes it highly suitable for real-time detection, as evidenced by its successful application in detecting Gly in orange juice and rice beverage samples. This demonstrates its efficacy for pesticide monitoring in practical food and environmental matrices. Similarly, Deller proposes a novel electrochemical sensor based on modified SPCE to quantify Pirimicarb (PMC), a carbamate pesticide that is challenging to detect electrochemically due to its high oxidation potential [165]. To enhance the electrochemical performance for PMC oxidation at low potential, SPCE was modified with conductive PEDOT and AuNPs. This modification enables the exploration of the correlation

between oxidation peak and pesticide concentration through an electrocatalytic effect, leading to the development of a sensitive, selective, and cost-effective electrochemical sensor for future environmental monitoring.

### 3.5. Toxic Gases

Humans are exposed to a wide range of air pollutants in both indoor and outdoor environments. Poor air quality is recognized as a trigger for various health issues that often result in life-threatening and costly emergency medical care [166]. Therefore, accurate detection of toxic gases would not only bring significant benefits to industries but also greatly improve the daily lives of individuals.

Ammonia is harmful to the respiratory system, skin and eyes, digestive system and nervous system, and also causes environmental pollution [167]. The PPy-based gas sensor for  $\text{NH}_3$  detection, developed by Jain, utilizes a combination of oxidizer and pyrrole to achieve exceptional thermal stability, superior electrical conductivity, and environmental stability [168]. The chemical oxidation polymerization method was employed to synthesize PPy in an aqueous solution, utilizing ferric chloride ( $\text{FeCl}_3$ ) as the oxidant and cetrimonium bromide as the solvent [169]. With the increase in the molar ratio of  $\text{FeCl}_3$  to pyrrole, the conductivity of PPy increased, and the conductivity of PPy was analyzed by I-V characteristics to get the optimal ratio. The influence of different concentrations of  $\text{NH}_3$  on the conductivity of PPy was used to achieve the detection of  $\text{NH}_3$ . While Bhardwaj prepared a three-phase Cu-MOF/graphene/PANI composite for  $\text{NH}_3$  sensing [170]. The three-phase composite has been synthesized in the presence of ammonium persulfate as an oxidizing agent. In this mixture, the aniline component undergoes polymerization to form PANI, which acts as a connecting bridge between Cu-MOF and graphene within the composite. The incorporation of Cu-MOF into the matrix facilitates the attainment of an electrochemically active sensing material possessing a surface area of approximately  $756 \text{ m}^2 \cdot \text{g}^{-1}$ , which is advantageous for  $\text{NH}_3$  diffusion. Moreover, this porous PANI-based sensor demonstrates remarkable sensitivity towards  $\text{NH}_3$  detection, exhibiting linear detection ranges spanning from 1 to 100 ppm and low detection limits of 0.6 ppm. In addition to PPy and PANI, PEDOT has also been utilized for the detection of  $\text{NH}_3$ . A high-performance chemically resistant  $\text{NH}_3$  sensor was developed by preparing an ultra-thin Janus film consisting of AuNWs/PEDOT-PSS double layers [171]. The AuNWs/PEDOT-PSS Janus film was fabricated by subjecting the AuNWs membrane to  $\text{H}_2\text{S}$  treatment, resulting in a hydrophilic surface, which was subsequently combined with a layer of PEDOT/PSS. The Janus film containing a single layer of AuNWs exhibited the most pronounced response to  $\text{NH}_3$ . Furthermore, as the thermal annealing treatment temperature increased within the range of 80 to 200 °C, the sensitivity towards  $\text{NH}_3$  also escalated due to the alteration in the state of AuNWs, leading to an enlargement in available surface area for  $\text{NH}_3$  adsorption. Significantly, this study introduces a novel approach for fabricating flexible, transparent, and conductive Janus films, thereby establishing a promising platform for electrochemical sensors.

$\text{H}_2\text{S}$  is a gaseous compound of hydrogen and sulfur, characterized by a potent odor and exhibiting toxic effects on the respiratory system, nervous system, and biomolecules in humans [172]. The biodegradable electroactive polymer, polyurethane-urea (PUU) and PUU-activated carbon (AC) composites were utilized as sensitive materials for successfully fabricate a high-performance  $\text{H}_2\text{S}$  sensor capable of operating at room temperature [173]. The PUU was synthesized through the copolymerization of biodegradable polycaprolactone diol and electroactive amine-coated aniline trimers, while the activated carbon was prepared from waste coconut shell. The investigation of PUU and AC was conducted in varying proportions, resulting in a higher sensitivity to  $\text{H}_2\text{S}$  gas when AC was added. It is hypothesized that the enhanced response of the PUU-AC composite to  $\text{H}_2\text{S}$  can be attributed to its elevated surface area and abundant reaction sites, which facilitate gas diffusion, adsorption, and electron transfer. The successful fabrication of interdigitated electrode (IDE) coated with PANI-AC composites enables the homoplastic detection of

H<sub>2</sub>S [174]. The PANI was synthesized through oxidative coupling polymerization of aniline monomers, while the AC was obtained by calcinating coconut husks from agricultural waste at 800 °C with ZnCl<sub>2</sub> as a catalyst. The superior gas-sensitive properties of PANI-AC composites can be attributed to the increased surface area, providing more active sites for doping and enhancing sensing capability. Specifically, incorporating AC into the PANI matrix significantly improves the doping process, resulting in a stronger response to H<sub>2</sub>S, higher repeatability, and greater stability compared to pure PANI-coated IDE sensors.

PANI is a potential material for electrochemical sensors because of its special physical and chemical characteristics, which include outstanding gas absorption, little dielectric loss, and exceptional durability in both chemical and thermal conditions. However, the sensing performance is highly dependent on the structure and size of PANI [175–177]. Although in situ oxidation polymerization combined with self-assembly processes has become the primary method for fabricating flexible PANI-based gas sensors, achieving a uniform array of microwires remains an urgent challenge that needs to be addressed. Zhao adopted a novel approach to fabricate one-dimensional PANI microwire arrays via the liquid film-induced capillary bridge method, utilizing an extremely low concentration of PANI solution [178]. The formation rate of PANI microwire can be significantly enhanced by employing a silicone template modified with hydrophobic 1H,1H,2H,2H perfluorodecyl triethoxysilane (PTES) (Figure 16). The PANI solution, with a concentration of  $1 \times 10^{12}$  pg·mL<sup>-1</sup> and a silicon template of 10 μm, was evaporated at 80 °C for 18 h, resulting in a 100% rate of PANI microwire formation. The obtained PANI microwires demonstrate uniformity in size and possess well-defined shapes, with respective widths and heights measuring 2 μm and 250 nm (Figure 16b). The prepared microwire array enables the detection of SO<sub>2</sub> at room temperature, exhibiting a response time of 20 s and a detection limit of 1 ppm. As a result, the liquid film-induced capillary bridge method offers an innovative opportunity for fabricating gas sensor devices based on insoluble polymers.

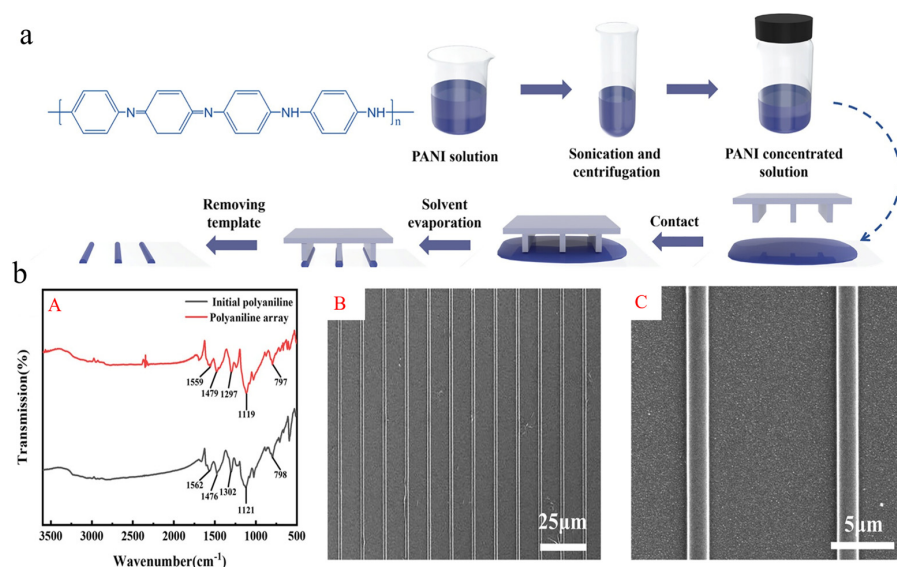


**Figure 16.** (a) Schematic diagram of PANI microwire array prepared by liquid film-induced capillary bridge method. (b) FTIR spectra of the initial PANI (black) and PANI array (red) (A). The FTIR spectra of the two samples were consistent, indicating that the PANI micron array was prepared by liquid film-induced capillary bridge method. SEM image of PANI array with microarrays arranged in parallel and evenly spaced (B). SEM image of PANI array after partial amplification (C). The edge of the microwire is straight and the width is uniform. Reprinted with permission from ref. [178].

Jang has created a highly sensitive OFET-based gas sensor to detect NO<sub>2</sub>. The conducting polymer poly (3-hexylthiophene)(P3HT) acts as a charge transport agent and is placed in a semiconductor layer with a field effect transistor (OFET) [179]. The surface chemistry

of the perovskite NCs is modified by ligand exchange treatment so that the NCs is encased in a photoionic polymer that strongly interacts not only with the surface of the perovskite NCs, but also with the target gas molecules (Figure 17). In addition, the researchers used hydrated perovskite NCs to optimize their ability to capture  $\text{NO}_2$  through interactions with water molecules and  $\text{NO}_2$ . These results demonstrate the potential of organic–inorganic hybrid sensors, which will provide a new approach for developing gas sensors based on composites of different materials, aimed at increasing sensitivity and selectivity.

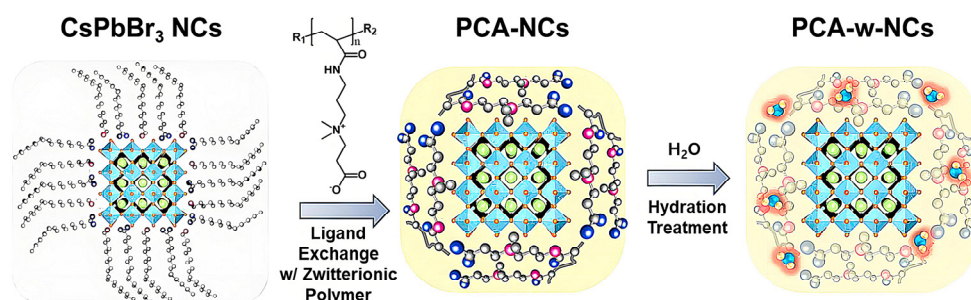


**Figure 17.** Schematic diagram of  $\text{CsPbBr}_3$  perovskite NCs being exchanged by polymer ligands. Reprinted with permission from ref. [179].

An updated comparative list of different CPs applications in environmental monitoring is presented in Table 2.

**Table 2.** The main electrochemical sensors based on CPs and their parameter analysis, the application of electrochemical technology and its application in environmental detection are introduced.

CPs	Analyte	LOD (mM)	Linear Range (mM)	Application	Ref.
PPy	nitrate	0.0537	0.0525–100	Nitrate nitrogen	[139]
PANI	nitrate	$9 \times 10^{-5}$	0.0008–0.03	Nitrate nitrogen	[141]
POT	nitrate	$2.1 \times 10^{-5}$	$1.61 \times 10^{-5}$ –24.19	Nitrate nitrogen	[142]
PEDOT	nitrate	$1.61 \times 10^{-5}$	$1.61 \times 10^{-5}$ –16.13	Nitrate nitrogen	[144]
PANI, PPy	$\text{Cd}^{2+}$ , $\text{Cu}^{2+}$ , $\text{Pb}^{2+}$ , $\text{Hg}^{2+}$	$2.608 \times 10^{-5}$ , $5.323 \times 10^{-5}$ , $1.484 \times 10^{-5}$ , $0.835 \times 10^{-5}$	0.0005–0.1, 0.001–0.1, 0.0001–0.1, 0.001–0.01	Heavy metal ions	[147]
PPy	$\text{Pb}^{2+}$	$3 \times 10^{-8}$	$10^{-7}$ – $10^{-3}$	Heavy metal ions	[149]
PANI	$\text{Pb}^{2+}$ , $\text{Hg}^{2+}$	$4.6 \times 10^{-9}$ , $10^{-9}$	0.001–0.0248	Heavy metal ions	[151]
PANI	$\text{Cd}^{2+}$ , $\text{Pb}^{2+}$	$6.85 \times 10^{-4}$ , $1.59 \times 10^{-4}$	$4.8 \times 10^{-6}$ – $1.02 \times 10^{-5}$ , $1.11 \times 10^{-3}$ – $1.93 \times 10^{-3}$	Heavy metal ions	[152]
PEDOT	$\text{Cd}^{2+}$ , $\text{Cu}^{2+}$ , $\text{Pb}^{2+}$	$5.78 \times 10^{-6}$ , $2.7 \times 10^{-6}$ , $1.7 \times 10^{-6}$	$4 \times 10^{-5}$ – $2.8 \times 10^{-3}$ , $2.4 \times 10^{-5}$ – $2.8 \times 10^{-3}$ , $1.6 \times 10^{-4}$ – $3.2 \times 10^{-3}$	Heavy metal ions	[153]
PANI	CEF	7.1	$2 \times 10^{-5}$ – $9.5 \times 10^{-5}$	Antibiotics	[158]
PTh	SAs	$1.7 \times 10^{-7}$	$1 \times 10^{-6}$ – $1 \times 10^{-2}$	Antibiotics	[155]
PANI	OXC	$2 \times 10^{-7}$	$7 \times 10^{-7}$ – $5.75 \times 10^{-4}$	Antibiotics	[156]
PANI	DMZ	$1.78 \times 10^{-6}$	$7.9 \times 10^{-4}$ –2.057	Antibiotics	[161]
PTh	CPF	0.04 nM	$2 \times 10^{-8}$ – $10^{-3}$	Pesticide	[163]
PPy	Gly	$7.12 \times 10^{-6}$	$9.18 \times 10^{-6}$ – $1.28 \times 10^{-3}$	Pesticide	[164]
PEDOT/PSS	PMC	0.02834	0.09381–0.75	Pesticide	[165]
PANI	$\text{NH}_3$	$3.52 \times 10^{-5}$	$5.87 \times 10^{-5}$ – $5.87 \times 10^{-3}$	Toxic gas	[170]
PEDOT/PSS	$\text{NH}_3$	$2.94 \times 10^{-5}$	$5.87 \times 10^{-4}$ – $5.87 \times 10^{-3}$	Toxic gas	[171]
PANI	$\text{H}_2\text{S}$	$5.87 \times 10^{-4}$	$2.93 \times 10^{-5}$ – $1.47 \times 10^{-4}$	Toxic gas	[173]
PANI	$\text{SO}_2$	$1.56 \times 10^{-5}$	$1.56 \times 10^{-5}$ – $7.8 \times 10^{-4}$	Toxic gas	[178]
P3HT	$\text{NO}_2$	$6.91 \times 10^{-12}$	$2.17 \times 10^{-4}$ – $2.17 \times 10^{-2}$	Toxic gas	[179]

#### 4. Summary and Prospect

Recent research has significantly advanced our understanding of the potential of CPs in electrochemical sensors, which holds great promise for revolutionizing current practices



in medical care and environmental monitoring by shifting the focus from traditional off-site laboratory analysis to in situ detection. CPs can be functionalized with diverse groups, enabling their transformation into a wide range of biometric molecules. Furthermore, integration with organic/inorganic nanomaterials enhances their sensitivity and selectivity in detecting biological analytes.

Although CPs-based electrochemical sensors have advantages in biomedical and environmental applications, there are still areas for improvement, such as CPs being affected by oxidation, hydrolysis, light, and other factors, resulting in limited stability and service life. Some CPs may be too sensitive to specific molecules under certain conditions, causing the presence of interfering substances to interfere with the accuracy of the sensor. Some CPs are difficult to regenerate or recycle, resulting in resource waste and environmental burden. Therefore, improving the reliability and applicability of electrochemical sensors is an important research field, which involves many aspects of optimization. In terms of improving sensitivity, the signal response of the sensor can be enhanced by optimizing the electrode design and material selection of the sensor. Increasing specificity requires selectively improving the properties of the target analyte, such as surface modifications or the introduction of molecular recognition elements. Long-term stability can be achieved by preventing contamination and oxidation of the electrode surface. In terms of biocompatibility, materials compatible with the organism should be selected to ensure the safe and reliable application of the sensor in the organism. In terms of practicality and portability, miniaturization technology and portable test platforms can be used to simplify the operation process and improve the ease of use. Finally, in terms of cost-effectiveness, costs can be reduced by optimizing material selection, the manufacturing process and production scale, thus promoting the commercialization and scale application of electrochemical sensors. It is believed that with the development of the CPs field, new conductive polymers can be designed to improve their stability, selectivity and repeatability to meet the needs of different application fields. Intelligent technologies such as artificial intelligence and machine learning can be combined to optimize sensor response and performance and improve accuracy and reliability. The development of multifunctional CPs capable of simultaneously detecting multiple target substances has improved the applicability and practicality of sensors. The preparation method of environmentally friendly CPs was studied to reduce energy consumption and environmental pollution and promote the sustainable development of electrochemical sensors. In the future, CPs have broad application prospects in the field of electrochemical sensors, but the field also needs continuous technological innovation and improvement to solve existing defects and meet the needs of future applications.

**Author Contributions:** Conceptualization, Y.P., J.Z. and X.G.; methodology, Y.L. and L.L.; investigation, Y.P., J.Z., X.G. and Y.L.; writing—original draft preparation, Y.P.; writing—review and editing, L.L. and L.P.; supervision, L.L. All authors have read and agreed to the published version of the manuscript.

**Funding:** This research was supported by the National Natural Science Foundation of China (No. 61904049, 61825403), the 14th Five-Year National Key Research and Development Project (No. 2021YFD1700904-04) and the Top Talent Program of Henan Agricultural University.

**Institutional Review Board Statement:** Not applicable.

**Informed Consent Statement:** Not applicable.

**Data Availability Statement:** Not applicable.

**Conflicts of Interest:** The authors declare no conflicts of interest.

## References

1. Zhao, Y.; Lei, M.; Liu, S.-X.; Zhao, Q. Smart hydrogel-based optical fiber SPR sensor for pH measurements. *Sens. Actuators B Chem.* **2018**, *261*, 226–232. [[CrossRef](#)]
2. Wencel, D.; Kaworek, A.; Abel, T.; Efremov, V.; Bradford, A.; Carthy, D.; Coady, G.; McMorro, R.C.N.; McDonagh, C. Optical Sensor for Real-Time pH Monitoring in Human Tissue. *Small* **2018**, *14*, 1803627. [[CrossRef](#)] [[PubMed](#)]

3. Safavi, A.; Bagheri, M. Novel optical pH sensor for high and low pH values. *Sens. Actuators B Chem.* **2003**, *90*, 143–150. [[CrossRef](#)]
4. Wang, J.; Xue, N.; Pan, W.; Tu, R.; Li, S.; Zhang, Y.; Mao, Y.; Liu, Y.; Cheng, H.; Guo, Y.; et al. Repurposing conformational changes in ANL superfamily enzymes to rapidly generate biosensors for organic and amino acids. *Nat. Commun.* **2023**, *14*, 6680. [[CrossRef](#)] [[PubMed](#)]
5. Hwang, H.G.; Ye, D.-Y.; Jung, G.Y. Biosensor-guided discovery and engineering of metabolic enzymes. *Biotechnol. Adv.* **2023**, *69*, 108251. [[CrossRef](#)] [[PubMed](#)]
6. Wu, R.; Li, L.; Pan, L.; Yan, K.; Shi, Y.; Jiang, L.; Zhu, J.-J. Long-term cell culture and electrically *in situ* monitoring of living cells based on a polyaniline hydrogel sensor. *J. Mater. Chem. B* **2021**, *9*, 9514–9523. [[CrossRef](#)] [[PubMed](#)]
7. Kim, H.J.; Park, D.; Park, Y.; Kim, D.-H.; Kim, J. Electric-Field-Mediated In-Sensor Alignment of Antibody's Orientation to Enhance the Antibody-Antigen Binding for Ultrahigh Sensitivity Sensors. *Nano Lett.* **2022**, *22*, 6537–6544. [[CrossRef](#)]
8. Stanford, M.G.; Yang, K.; Chyan, Y.; Kittrell, C.; Tour, J.M. Laser-Induced Graphene for Flexible and Embeddable Gas Sensors. *ACS Nano* **2019**, *13*, 3474–3482. [[CrossRef](#)]
9. Tang, W.; Chen, Z.; Song, Z.; Wang, C.; Wan, Z.; Chan, C.L.J.; Chen, Z.; Ye, W.; Fan, Z. Microheater Integrated Nanotube Array Gas Sensor for Parts-Per-Trillion Level Gas Detection and Single Sensor-Based Gas Discrimination. *ACS Nano* **2022**, *16*, 10968–10978. [[CrossRef](#)]
10. Zhang, H.; Li, Y.; Zhang, Y.; Wu, J.; Hu, J.; Li, S.; Li, L. Simultaneous detection of lead and cadmium based on N-doped MoS<sub>2</sub>/MWCNTs nanocomposites. *J. Mater. Sci.* **2023**, *58*, 6643–6655. [[CrossRef](#)]
11. Yang, T.; Yu, R.; Yan, Y.; Zeng, H.; Luo, S.; Liu, N.; Morrin, A.; Luo, X.; Li, W. A review of ratiometric electrochemical sensors: From design schemes to future prospects. *Sens. Actuators B Chem.* **2018**, *274*, 501–516. [[CrossRef](#)]
12. Yang, G.; Zhao, F. Electrochemical sensor for dimetridazole based on novel gold nanoparticles@molecularly imprinted polymer. *Sens. Actuators B Chem.* **2015**, *220*, 1017–1022. [[CrossRef](#)]
13. Maduraiveeran, G.; Ramaraj, R. A facile electrochemical sensor designed from gold nanoparticles embedded in three-dimensional sol-gel network for concurrent detection of toxic chemicals. *Electrochem. Commun.* **2007**, *9*, 2051–2055. [[CrossRef](#)]
14. Pan, L.; Yu, G.; Zhai, D.; Lee, H.R.; Zhao, W.; Liu, N.; Wang, H.; Tee, B.C.K.; Shi, Y.; Cui, Y.; et al. Hierarchical nanostructured conducting polymer hydrogel with high electrochemical activity. *Proc. Natl. Acad. Sci. USA* **2012**, *109*, 9287–9292. [[CrossRef](#)] [[PubMed](#)]
15. Wang, J.; Timchalk, C.; Lin, Y. Carbon nanotube-based electrochemical sensor for assay of salivary cholinesterase enzyme activity: An exposure biomarker of organophosphate pesticides and nerve agents. *Environ. Sci. Technol.* **2008**, *42*, 2688–2693. [[CrossRef](#)] [[PubMed](#)]
16. Liu, R.; Li, B.; Li, F.; Dubovyk, V.; Chang, Y.; Li, D.; Ding, K.; Ran, Q.; Wang, G.; Zhao, H. A novel electrochemical sensor based on  $\beta$ -cyclodextrin functionalized carbon nanosheets@carbon nanotubes for sensitive detection of bactericide carbendazim in apple juice. *Food Chem.* **2022**, *384*, 132573. [[CrossRef](#)] [[PubMed](#)]
17. Meng, F.; Duan, M.; Wu, W.; Shao, S.; Qin, Y.; Zhang, M. Enzymatic construction Au NPs-rGO based MIP electrochemical sensor for adulteration detection of bovine-derived allergen in camel milk. *Food Chem.* **2024**, *436*, 137638. [[CrossRef](#)] [[PubMed](#)]
18. Yang, G.; Zhao, F. Electrochemical sensor for chloramphenicol based on novel multiwalled carbon nanotubes@molecularly imprinted polymer. *Biosens. Bioelectron.* **2015**, *64*, 416–422. [[CrossRef](#)] [[PubMed](#)]
19. Chiang, C.K.; Fincher, C.R.; Park, Y.W.; Heeger, A.J.; Shirakawa, H.; Louis, E.J.; Gau, S.C.; MacDiarmid, A.G. Electrical Conductivity in Doped Polyacetylene. *Phys. Rev. Lett.* **1977**, *39*, 1098–1101. [[CrossRef](#)]
20. Le, T.-H.; Kim, Y.; Yoon, H. Electrical and Electrochemical Properties of Conducting Polymers. *Polymers* **2017**, *9*, 150. [[CrossRef](#)]
21. Tsukamoto, J.; Takahashi, A.; Kawasaki, K. Structure and Electrical Properties of Polyacetylene Yielding a Conductivity of 105 S/cm. *Jpn. J. Appl. Phys.* **1990**, *29*, 125. [[CrossRef](#)]
22. Dong, Y.; Liu, C.; Li, F.; Jin, H.; Li, B.; Ding, F.; Yang, Y.; Yang, Z.; Yuan, F. Highly Conductive Ultrafine N-Doped Silicon Powders Prepared by High-Frequency Thermal Plasma and Their Application as Anodes for Lithium-Ion Batteries. *ACS Appl. Electron. Mater.* **2023**, *6*, 816–827. [[CrossRef](#)]
23. Boosagulla, D.; Mandati, S.; Allikayala, R.; Sarada, B.V. Growth mechanism of pulse electrodeposited cadmium sulfide and zinc sulfide thin films with tartaric acid and glycerol as additives. *Thin Solid Films* **2022**, *741*, 139011. [[CrossRef](#)]
24. Aguilar-Bolados, H.; Vargas-Astudillo, D.; Yazdani-Pedram, M.; Acosta-Villavicencio, G.; Fuentealba, P.; Contreras-Cid, A.; Verdejo, R.; Lopez-Manchado, M.A. Facile and Scalable One-Step Method for Amination of Graphene Using Leuckart Reaction. *Chem. Mater.* **2017**, *29*, 6698–6705. [[CrossRef](#)]
25. Bi, S.; Hou, L.; Lu, Y. Multifunctional sodium alginate fabric based on reduced graphene oxide and polypyrrole for wearable closed-loop point-of-care application. *Chem. Eng. J.* **2021**, *406*, 126778. [[CrossRef](#)]
26. Xia, J.; Chen, L.; Yanagida, S. Application of polypyrrole as a counter electrode for a dye-sensitized solar cell. *J. Mater. Chem.* **2011**, *21*, 4644–4649. [[CrossRef](#)]
27. Thadathil, A.; Pradeep, H.; Joshy, D.; Ismail, Y.A.; Periyat, P. Polyindole and polypyrrole as a sustainable platform for environmental remediation and sensor applications. *Mater. Adv.* **2022**, *3*, 2990–3022. [[CrossRef](#)]
28. Yang, P.; Mai, W. Flexible solid-state electrochemical supercapacitors. *Nano Energy* **2014**, *8*, 274–290. [[CrossRef](#)]
29. Chen, J.; Feng, J.; Yan, W. Influence of metal oxides on the adsorption characteristics of PPy/metal oxides for Methylene Blue. *J. Colloid Interface Sci.* **2016**, *475*, 26–35. [[CrossRef](#)]

30. Zare, E.N.; Makvandi, P.; Ashtari, B.; Rossi, F.; Motahari, A.; Perale, G. Progress in Conductive Polyaniline-Based Nanocomposites for Biomedical Applications: A Review. *J. Med. Chem.* **2020**, *63*, 1–22. [[CrossRef](#)]
31. Li, L.; Shi, Y.; Pan, L.; Shi, Y.; Yu, G. Additional Article Notification: Rational design and applications of conducting polymer hydrogels as electrochemical biosensors. *J. Mater. Chem. B* **2015**, *3*, 5111–5121. [[CrossRef](#)] [[PubMed](#)]
32. Li, Y.; Wu, J.; Zhang, H.; Hu, J.; Li, S.; Li, L. An all-solid-state ion-selective sensor based on polyaniline for nitrate-nitrogen detection. *J. Mater. Sci.* **2023**, *58*, 17292–17302. [[CrossRef](#)]
33. Chaudhary, A.; Pathak, D.K.; Tanwar, M.; Yogi, P.; Sagdeo, P.R.; Kumar, R. Polythiophene-PCBM-Based All-Organic Electrochromic Device: Fast and Flexible. *ACS Appl. Electron. Mater.* **2019**, *1*, 58–63. [[CrossRef](#)]
34. Kaloni, T.P.; Giesbrecht, P.K.; Schreckenbach, G.; Freund, M.S. Polythiophene: From Fundamental Perspectives to Applications. *Chem. Mater.* **2017**, *29*, 10248–10283. [[CrossRef](#)]
35. Thanasamy, D.; Jesuraj, D.; Kannan, S.K.K.; Avadhanam, V. A novel route to synthesis polythiophene with great yield and high electrical conductivity without post doping process. *Polymer* **2019**, *175*, 32–40. [[CrossRef](#)]
36. Chen, R.; Chen, S.; Zhou, Y.; Wei, Z.; Wang, H.; Zheng, Y.; Li, M.; Sun, K.; Li, Y. Unsubstituted Polythiophene Film Deposited via In-Situ Sequential Solution Polymerization for Chemo-/Electrochromism. *Macromolecules* **2020**, *53*, 4247–4254. [[CrossRef](#)]
37. Serrano-Garcia, W.; Bonadies, I.; Thomas, S.; Guarino, V. P3HT loaded piezoelectric electrospun fibers for tunable molecular adsorption. *Mater. Lett.* **2020**, *266*, 127458. [[CrossRef](#)]
38. Agbolaghi, S.; Zenoozi, S. A comprehensive review on poly(3-alkylthiophene)-based crystalline structures, protocols and electronic applications. *Org. Electron.* **2017**, *51*, 362–403. [[CrossRef](#)]
39. Wang, Y.; Li, Z.; Sun, D.; Jiang, N.; Niu, K.; Giuntoli, A.; Xia, W. Understanding the thermomechanical behavior of graphene-reinforced conjugated polymer nanocomposites via coarse-grained modeling. *Nanoscale* **2023**, *15*, 17124–17137. [[CrossRef](#)]
40. Gadisa, A.; Oosterbaan, W.D.; Vandewal, K.; Bolsee, J.-C.; Bertho, S.; D'Haen, J.; Lutsen, L.; Vanderzande, D.; Manca, J.V. Effect of Alkyl Side-Chain Length on Photovoltaic Properties of Poly(3-alkylthiophene)/PCBM Bulk Heterojunctions. *Adv. Funct. Mater.* **2009**, *19*, 3300–3306. [[CrossRef](#)]
41. Wang, H.-J.; Tzeng, J.-Y.; Chou, C.-W.; Huang, C.-Y.; Lee, R.-H.; Jeng, R.-J. Novel polythiophene derivatives functionalized with conjugated side-chain pendants comprising triphenylamine/carbazole moieties for photovoltaic cell applications. *Polym. Chem.* **2013**, *4*, 506–519. [[CrossRef](#)]
42. Razzell-Hollis, J.; Fleischli, F.; Jahnke, A.A.; Stingelin, N.; Seferos, D.S.; Kim, J.-S. Effects of Side-Chain Length and Shape on Polytellurophene Molecular Order and Blend Morphology. *J. Phys. Chem. C* **2017**, *121*, 2088–2098. [[CrossRef](#)]
43. Nejati, S.; Minford, T.E.; Smolin, Y.Y.; Lau, K.K.S. Enhanced Charge Storage of Ultrathin Polythiophene Films within Porous Nanostructures. *ACS Nano* **2014**, *8*, 5413–5422. [[CrossRef](#)] [[PubMed](#)]
44. Yang, Y.; Deng, H.; Fu, Q. Recent progress on PEDOT:PSS based polymer blends and composites for flexible electronics and thermoelectric devices. *Mater. Chem. Front.* **2020**, *4*, 3130–3152. [[CrossRef](#)]
45. Fan, X.; Nie, W.; Tsai, H.; Wang, N.; Huang, H.; Cheng, Y.; Wen, R.; Ma, L.; Yan, F.; Xia, Y. PEDOT:PSS for Flexible and Stretchable Electronics: Modifications, Strategies, and Applications. *Adv. Sci.* **2019**, *6*, 1900813. [[CrossRef](#)] [[PubMed](#)]
46. Kim, Y.H.; Sachse, C.; Machala, M.L.; May, C.; Mueller-Meskamp, L.; Leo, K. Highly Conductive PEDOT:PSS Electrode with Optimized Solvent and Thermal Post-Treatment for ITO-Free Organic Solar Cells. *Adv. Funct. Mater.* **2011**, *21*, 1076–1081. [[CrossRef](#)]
47. Wu, F.; Li, P.; Sun, K.; Zhou, Y.; Chen, W.; Fu, J.; Li, M.; Lu, S.; Wei, D.; Tang, X.; et al. Conductivity Enhancement of PEDOT:PSS via Addition of Chloroplatinic Acid and Its Mechanism. *Adv. Electron. Mater.* **2017**, *3*, 1700047. [[CrossRef](#)]
48. Wang, C.; Sun, K.; Fu, J.; Chen, R.; Li, M.; Zang, Z.; Liu, X.; Li, B.; Gong, H.; Ouyang, I. Enhancement of Conductivity and Thermoelectric Property of PEDOT:PSS via Acid Doping and Single Post-Treatment for Flexible Power Generator. *Adv. Sustain. Syst.* **2018**, *2*, 1800085. [[CrossRef](#)]
49. Zhang, L.; Yang, K.; Chen, R.; Zhou, Y.; Chen, S.; Zheng, Y.; Li, M.; Xu, C.; Tang, X.; Zang, Z.; et al. The Role of Mineral Acid Doping of PEDOT:PSS and Its Application in Organic Photovoltaics. *Adv. Electron. Mater.* **2020**, *6*, 1900648. [[CrossRef](#)]
50. Bessaire, B.; Mathieu, M.; Salles, V.; Yeghoyan, T.; Celle, C.; Simonato, J.-P.; Brioude, A. Synthesis of Continuous Conductive PEDOT:PSS Nanofibers by Electrospinning: A Conformal Coating for Optoelectronics. *ACS Appl. Mater. Interfaces* **2017**, *9*, 950–957. [[CrossRef](#)]
51. Lim, H.C.; Jang, S.-J.; Cho, Y.; Cho, H.; Prasad, G.V.; Venkatachalam, V.; Shin, I.-S.; Kim, T.H. Graphene Quantum Dot-Doped PEDOT for Simultaneous Determination of Ascorbic Acid, Dopamine, and Uric Acid. *ChemElectroChem* **2022**, *9*, e202200557. [[CrossRef](#)]
52. Miao, Z.; Gonsales, S.A.; Ehm, C.; Mentink-Vigier, F.; Bowers, C.R.; Sumerlin, B.S.; Veige, A.S. Cyclic polyacetylene. *Nat. Chem.* **2021**, *13*, 792–799. [[CrossRef](#)] [[PubMed](#)]
53. Szuwarzynski, M.; Wolski, K.; Zapotoczny, S. Enhanced stability of conductive polyacetylene in ladder-like surface-grafted brushes. *Polym. Chem.* **2016**, *7*, 5664–5670. [[CrossRef](#)]
54. Shi, Y.; Peng, L.; Ding, Y.; Zhao, Y.; Yu, G. Nanostructured conductive polymers for advanced energy storage. *Chem. Soc. Rev.* **2015**, *44*, 6684–6696. [[CrossRef](#)] [[PubMed](#)]
55. Bhadra, S.; Khastgir, D.; Singha, N.K.; Lee, J.H. Progress in preparation, processing and applications of polyaniline. *Prog. Polym. Sci.* **2009**, *34*, 783–810. [[CrossRef](#)]

56. Bujak, P.; Kulszewicz-Bajer, I.; Zagorska, M.; Maurel, V.; Wielgus, I.; Pron, A. Polymers for electronics and spintronics. *Chem. Soc. Rev.* **2013**, *42*, 8895–8999. [[CrossRef](#)] [[PubMed](#)]
57. Hao, Z.; Zhang, J.; Xie, M.; Li, X.; Wang, L.; Liu, Y.; Niu, K.; Wang, J.; Song, L.; Cheng, T.; et al. From n-alkane to polyacetylene on Cu (110): Linkage modulation in chain growth. *Sci. China Chem.* **2022**, *65*, 733–739. [[CrossRef](#)]
58. Wang, S.; Hu, D.; Guan, X.; Cai, S.; Shi, G.; Shuai, Z.; Zhang, J.; Peng, Q.; Wan, X. Brightening up Circularly Polarized Luminescence of Monosubstituted Polyacetylene by Conformation Control: Mechanism, Switching, and Sensing. *Angew. Chem. Int. Ed.* **2021**, *60*, 21918–21926. [[CrossRef](#)] [[PubMed](#)]
59. Namsheer, K.; Rout, C.S. Conducting polymers: A comprehensive review on recent advances in synthesis, properties and applications. *RSC Adv.* **2021**, *11*, 5659–5697. [[CrossRef](#)]
60. Hu, X.; Wang, P.; Yang, J.; Zhang, B.; Li, J.; Luo, J.; Wu, K. Enhanced electrochemical detection of erythromycin based on acetylene black nanoparticles. *Colloids Surf. B Biointerfaces* **2010**, *81*, 27–31. [[CrossRef](#)]
61. Li, M.; Qi, Y.; Ding, Y.; Zhao, Q.; Fei, J.; Zhou, J. Electrochemical sensing platform based on the quaternized cellulose nanoparticles/acetylene black/enzymes composite film. *Sens. Actuators B Chem.* **2012**, *168*, 329–335. [[CrossRef](#)]
62. Tsou, T.-Y.; Lee, C.-Y.; Chiu, H.-T. K and Au Bicalyst Assisted Growth of Carbon Nanocoils from Acetylene: Effect of Deposition Parameters on Field Emission Properties. *ACS Appl. Mater. Interfaces* **2012**, *4*, 6505–6511. [[CrossRef](#)] [[PubMed](#)]
63. Sobczak, Q.; Kunche, A.; Magis, D.; Carrizo, D.S.; Miqueu, K.; Sotiropoulos, J.-M.; Cloutet, E.; Brochon, C.; Landais, Y.; Taton, D.; et al. Direct and selective access to amino-poly(phenylene vinylenes)s with switchable properties by dimerizing polymerization of aminoaryl carbenes. *Nat. Commun.* **2021**, *12*, 4093. [[CrossRef](#)] [[PubMed](#)]
64. Van der Zee, B.; Li, Y.; Wetzelaer, G.-J.A.H.; Blom, P.W.M. Efficiency of Polymer Light-Emitting Diodes: A Perspective. *Adv. Mater.* **2022**, *34*, 2108887. [[CrossRef](#)]
65. Malte, H.; Wang, T. Climate change: The rise in atmospheric CO<sub>2</sub> poses no risk for acid-base balance in humans. *Acta Physiol.* **2024**, *240*, e14066. [[CrossRef](#)] [[PubMed](#)]
66. Aoi, W.; Marunaka, Y. Importance of pH Homeostasis in Metabolic Health and Diseases: Crucial Role of Membrane Proton Transport. *Biomed Res. Int.* **2014**, *2014*, 598986. [[CrossRef](#)] [[PubMed](#)]
67. Sharma, V.K. The Future Is Wireless: Advances in Wireless Diagnostic and Therapeutic Technologies in Gastroenterology. *Gastroenterology* **2009**, *137*, 434–439. [[CrossRef](#)] [[PubMed](#)]
68. Abuhelwa, A.Y.; Foster, D.J.R.; Upton, R.N. A Quantitative Review and Meta-Models of the Variability and Factors Affecting Oral Drug Absorption-Part I: Gastrointestinal pH. *Aaps J.* **2016**, *18*, 1309–1321. [[CrossRef](#)] [[PubMed](#)]
69. Hajjar, S.; Zhou, X. pH sensing at the intersection of tissue homeostasis and inflammation. *Trends Immunol.* **2023**, *44*, 807–825. [[CrossRef](#)]
70. Parrilla, M.; Vanhooydonck, A.; Johns, M.; Watts, R.; De Wael, K. 3D-printed microneedle-based potentiometric sensor for pH monitoring in skin interstitial fluid. *Sens. Actuators B Chem.* **2023**, *378*, 133159. [[CrossRef](#)]
71. Power, G.; Moore, Z.; O'Connor, T. Measurement of pH, exudate composition and temperature in wound healing: A systematic review. *J. Wound Care* **2017**, *26*, 381–397. [[CrossRef](#)] [[PubMed](#)]
72. Abu Zahed, M.; Barman, S.C.; Das, P.S.; Sharifuzzaman, M.; Yoon, H.S.; Yoon, S.H.; Park, J.Y. Highly flexible and conductive poly (3, 4-ethylene dioxythiophene)-poly (styrene sulfonate) anchored 3-dimensional porous graphene network-based electrochemical biosensor for glucose and pH detection in human perspiration. *Biosens. Bioelectron.* **2020**, *160*, 112220. [[CrossRef](#)] [[PubMed](#)]
73. Zhu, C.; Xue, H.; Zhao, H.; Fei, T.; Liu, S.; Chen, Q.; Gao, B.; Zhang, T. A dual-functional polyaniline film-based flexible electrochemical sensor for the detection of pH and lactate in sweat of the human body. *Talanta* **2022**, *242*, 123289. [[CrossRef](#)] [[PubMed](#)]
74. Xu, Z.; Qiao, X.; Tao, R.; Li, Y.; Zhao, S.; Cai, Y.; Luo, X. A wearable sensor based on multifunctional conductive hydrogel for simultaneous accurate pH and tyrosine monitoring in sweat. *Biosens. Bioelectron.* **2023**, *234*, 115360. [[CrossRef](#)] [[PubMed](#)]
75. Simmer, P.; Li, S.K.; Kasting, G.; Heikenfeld, J. Prolonged and localized sweat stimulation by iontophoretic delivery of the slowly-metabolized cholinergic agent carbachol. *J. Dermatol. Sci.* **2018**, *89*, 40–51. [[CrossRef](#)] [[PubMed](#)]
76. Kim, J.; Jeerapan, I.; Imani, S.; Cho, T.N.; Bandonkar, A.; Cinti, S.; Mercier, P.P.; Wang, J. Noninvasive Alcohol Monitoring Using a Wearable Tattoo-Based Iontophoretic-Biosensing System. *ACS Sens.* **2016**, *1*, 1011–1019. [[CrossRef](#)]
77. Schmidt, A.M. Recent Highlights of ATVB Diabetes Mellitus. *Arterioscler. Thromb. Vasc. Biol.* **2014**, *34*, 954–958. [[CrossRef](#)] [[PubMed](#)]
78. Yeung, R.O.; Hannah-Shmouni, F.; Niederhoffer, K.; Walker, M.A. Not quite type 1 or type 2, what now? Review of monogenic, mitochondrial, and syndromic diabetes. *Rev. Endocr. Metab. Disord.* **2018**, *19*, 35–52. [[CrossRef](#)] [[PubMed](#)]
79. Li, N.; Liu, J.; Zhang, C.; Liu, G.; Leng, J.; Wang, L.; Li, W.; Yu, Z.; Hu, G.; Chan, J.C.N.; et al. Effects of lifestyle intervention during pregnancy on postpartum diabetes among Chinese women with gestational diabetes. *Diabetologia* **2021**, *64*, 255–258. [[CrossRef](#)]
80. Powers, M.A.; Marrero, D.G. Diabetes Self-management Education and Support in Type 2 Diabetes: A Joint Position Statement of the American Diabetes Association, the American Association of Diabetes Educators, and the Academy of Nutrition and Dietetics. *Diabetes Care* **2015**; *38*:1372–1382. *Diabetes Care* **2016**, *39*, E17. [[CrossRef](#)]
81. Yeon, S.Y.; Seo, M.; Kim, Y.; Hong, H.; Chung, T.D. Paper-based electrochromic glucose sensor with polyaniline on indium tin oxide nanoparticle layer as the optical readout. *Biosens. Bioelectron.* **2022**, *203*, 114002. [[CrossRef](#)] [[PubMed](#)]
82. Chen, T.-L.; Lo, Y.-L.; Liao, C.-C.; Quoc-Hung, P. Noninvasive measurement of glucose concentration on human fingertip by optical coherence tomography. *J. Biomed. Opt.* **2018**, *23*, 047001. [[CrossRef](#)] [[PubMed](#)]

83. Kong, D.-D.; Han, T.-S.; Ge, Q.; Chen, W.-L.; Liu, R.; Li, C.-X.; Xu, K.-X. Verification of Signal Extraction Capability of Near-Infrared Non-Invasive Blood Glucose Detection System. *Spectrosc. Spectr. Anal.* **2020**, *40*, 3438–3442. [[CrossRef](#)]
84. Karpova, E.V.; Karyakin, A.A. Noninvasive monitoring of diabetes and hypoxia by wearable flow-through biosensors. *Curr. Opin. Electrochem.* **2020**, *23*, 16–20. [[CrossRef](#)]
85. Khan, A.; Khan, A.A.P.; Marwani, H.M.; Alotaibi, M.M.; Asiri, A.M.; Manikandan, A.; Siengchin, S.; Rangappa, S.M. Sensitive Non-Enzymatic Glucose Electrochemical Sensor Based on Electrochemically Synthesized PANI/Bimetallic Oxide Composite. *Polymers* **2022**, *14*, 3047. [[CrossRef](#)] [[PubMed](#)]
86. Zhai, D.; Liu, B.; Shi, Y.; Pan, L.; Wang, Y.; Li, W.; Zhang, R.; Yu, G. Highly Sensitive Glucose Sensor Based on Pt Nanoparticle/Polyaniline Hydrogel Heterostructures. *ACS Nano* **2013**, *7*, 3540–3546. [[CrossRef](#)] [[PubMed](#)]
87. Li, L.; Pan, L.; Ma, Z.; Yan, K.; Cheng, W.; Shi, Y.; Yu, G. All Inkjet-Printed Amperometric Multiplexed Biosensors Based on Nanostructured Conductive Hydrogel Electrodes. *Nano Lett.* **2018**, *18*, 3322–3327. [[CrossRef](#)] [[PubMed](#)]
88. Pan, Y.; He, M.; Wu, J.; Qi, H.; Cheng, Y. One-step synthesis of MXene-functionalized PEDOT:PSS conductive polymer hydrogels for wearable and noninvasive monitoring of sweat glucose. *Sens. Actuators B Chem.* **2024**, *401*, 135055. [[CrossRef](#)]
89. GhavamiNejad, P.; GhavamiNejad, A.; Zheng, H.; Dhingra, K.; Samarikhalaj, M.; Poudineh, M. A Conductive Hydrogel Microneedle-Based Assay Integrating PEDOT:PSS and Ag-Pt Nanoparticles for Real-Time, Enzyme-Less, and Electrochemical Sensing of Glucose. *Adv. Healthc. Mater.* **2023**, *12*, 2202362. [[CrossRef](#)]
90. Vitali, C.; Remaley, A.T.; Cuchel, M. Is Low-Density Lipoprotein Cholesterol the Key to Interpret the Role of Lecithin:Cholesterol Acyltransferase in Atherosclerosis? *Circulation* **2018**, *138*, 1008–1011. [[CrossRef](#)]
91. Garland, M.R.; Hallahan, B.; McNamara, M.; Carney, P.A.; Grimes, H.; Hibbeln, J.R.; Harkin, A.; Conroy, R.M. Lipids and essential fatty acids in patients presenting with self-harm. *Br. J. Psychiatry* **2007**, *190*, 112–117. [[CrossRef](#)] [[PubMed](#)]
92. Bibbins-Domingo, K.; Grossman, D.C.; Curry, S.J.; Davidson, K.W.; Epling, J.W., Jr.; Garcia, F.A.R.; Gillman, M.W.; Kemper, A.R.; Krist, A.H.; Kurth, A.E.; et al. Screening for Lipid Disorders in Children and Adolescents US Preventive Services Task Force Recommendation Statement. *JAMA J. Am. Med. Assoc.* **2016**, *316*, 625–633. [[CrossRef](#)] [[PubMed](#)]
93. Tuteja, S.; Rader, D.J. DYSLIPIDAEMIA Cardiovascular prevention-end of the road for niacin? *Nat. Rev. Endocrinol.* **2014**, *10*, 646–647. [[CrossRef](#)] [[PubMed](#)]
94. Gudzone, K.A.; Monroe, A.K.; Sharma, R.; Ranasinghe, P.D.; Chelladurai, Y.; Robinson, K.A. Effectiveness of Combination Therapy With Statin and Another Lipid-Modifying Agent Compared With Intensified Statin Monotherapy A Systematic Review. *Ann. Intern. Med.* **2014**, *160*, 468–476. [[CrossRef](#)] [[PubMed](#)]
95. Alagappan, M.; Immanuel, S.; Sivasubramanian, R.; Kandaswamy, A. Development of cholesterol biosensor using Au nanoparticles decorated f-MWCNT covered with polypyrrole network. *Arab. J. Chem.* **2020**, *13*, 2001–2010. [[CrossRef](#)]
96. Li, L.; Wang, Y.; Pan, L.; Shi, Y.; Cheng, W.; Shi, Y.; Yu, G. A Nanostructured Conductive Hydrogels-Based Biosensor Platform for Human Metabolite Detection. *Nano Lett.* **2015**, *15*, 1146–1151. [[CrossRef](#)] [[PubMed](#)]
97. Thivya, P.; Ramya, R.; Wilson, J. Poly(3,4-ethylenedioxythiophene)/taurine biocomposite on screen printed electrode: Non-enzymatic cholesterol biosensor. *Microchem. J.* **2020**, *157*, 105037. [[CrossRef](#)]
98. Wan, Y.; Wang, P.; Su, Y.; Wang, L.; Pan, D.; Aldalbahi, A.; Yang, S.; Zuo, X. Nanoprobe-Initiated Enzymatic Polymerization for Highly Sensitive Electrochemical DNA Detection. *ACS Appl. Mater. Interfaces* **2015**, *7*, 25618–25623. [[CrossRef](#)]
99. Yang, W.; Gerasimov, J.Y.; Lai, R.Y. Folding-based electrochemical DNA sensor fabricated on a gold-plated screen-printed carbon electrode. *Chem. Commun.* **2009**, *20*, 2902–2904. [[CrossRef](#)]
100. Wang, C.; Yuan, X.; Liu, X.; Gao, Q.; Qi, H.; Zhang, C. Signal-on impedimetric electrochemical DNA sensor using dithiothreitol modified gold nanoparticle tag for highly sensitive DNA detection. *Anal. Chim. Acta* **2013**, *799*, 36–43. [[CrossRef](#)]
101. Lubin, A.A.; Lai, R.Y.; Baker, B.R.; Heeger, A.J.; Plaxco, K.W. Sequence-specific, electronic detection of oligonucleotides in blood, soil, and foodstuffs with the reagentless, reusable E-DNA sensor. *Anal. Chem.* **2006**, *78*, 5671–5677. [[CrossRef](#)] [[PubMed](#)]
102. Xu, W.; Jin, T.; Dai, Y.; Liu, C.C. Surpassing the detection limit and accuracy of the electrochemical DNA sensor through the application of CRISPR Cas systems. *Biosens. Bioelectron.* **2020**, *155*, 112100. [[CrossRef](#)] [[PubMed](#)]
103. Wang, W.; Song, L.; Gao, Q.; Qi, H.; Zhang, C. Highly sensitive detection of DNA using an electrochemical DNA sensor with thionine-capped DNA/gold nanoparticle conjugates as signal tags. *Electrochem. Commun.* **2013**, *34*, 18–21. [[CrossRef](#)]
104. Kiransan, K.D.; Topcu, E. Conducting Polymer-Reduced Graphene Oxide Sponge Electrode for Electrochemical Detection Based on DNA Hybridization. *ACS Appl. Nano Mater.* **2020**, *3*, 5449–5462. [[CrossRef](#)]
105. Yang, L.; Wang, H.; Lue, H.; Hui, N. Phytic acid functionalized antifouling conducting polymer hydrogel for electrochemical detection of microRNA. *Anal. Chim. Acta* **2020**, *1124*, 104–112. [[CrossRef](#)] [[PubMed](#)]
106. Wang, Z.; Huang, Y.; Xu, K.; Zhong, Y.; He, C.; Jiang, L.; Sun, J.; Rao, Z.; Zhu, J.; Huang, J.; et al. Natural oxidase-mimicking copper-organic frameworks for targeted identification of ascorbate in sensitive sweat sensing. *Nat. Commun.* **2023**, *14*, 69. [[CrossRef](#)] [[PubMed](#)]
107. Xia, L.; Han, M.-J.; Zhou, L.; Huang, A.; Yang, Z.; Wang, T.; Li, F.; Yu, L.; Tian, C.; Zang, Z.; et al. S-Click Reaction for Isotropic Orientation of Oxidases on Electrodes to Promote Electron Transfer at Low Potentials. *Angew. Chem. Int. Ed.* **2019**, *58*, 16480–16484. [[CrossRef](#)] [[PubMed](#)]
108. Lei, Y.; Butler, D.; Lucking, M.C.; Zhang, F.; Xia, T.; Fujisawa, K.; Granzier-Nakajima, T.; Cruz-Silva, R.; Endo, M.; Terrones, H.; et al. Single-atom doping of MoS<sub>2</sub> with manganese enables ultrasensitive detection of dopamine: Experimental and computational approach. *Sci. Adv.* **2020**, *6*, eabc4250. [[CrossRef](#)] [[PubMed](#)]

109. Mugo, S.M.; Robertson, S.V.; Lu, W. A molecularly imprinted electrochemical microneedle sensor for multiplexed metabolites detection in human sweat. *Talanta* **2023**, *259*, 124531. [[CrossRef](#)]
110. Zhang, Q.; Xie, X.; Peng, J.; Chen, F.; Ma, J.; Li, C.; Liu, H.; Wang, D.; Wang, J. Direct C4-Acetoxylation of Tryptophan and Tryptophan-Containing Peptides via Palladium(II)-Catalyzed C-H Activation. *Org. Lett.* **2021**, *23*, 4699–4704. [[CrossRef](#)]
111. Koper, J.E.B.; Troise, A.D.; Loonen, L.M.P.; Vitaglione, P.; Capuano, E.; Fogliano, V.; Wells, J.M. Tryptophan Supplementation Increases the Production of Microbial-Derived AhR Agonists in an In Vitro Simulator of Intestinal Microbial Ecosystem. *J. Agric. Food Chem.* **2022**, *70*, 3958–3968. [[CrossRef](#)] [[PubMed](#)]
112. Xu, Z.; Liu, Y.; Lv, M.; Qiao, X.; Fan, G.-C.; Luo, X. An anti-fouling wearable molecular imprinting sensor based on semi-interpenetrating network hydrogel for the detection of tryptophan in sweat. *Anal. Chim. Acta* **2023**, *1283*, 341948. [[CrossRef](#)] [[PubMed](#)]
113. Bansal, R.; Hald, N.; Garcia-Segura, S. Towards the design of mechanical flexible electrodes for sensing: Self-standing polypyrrole-copper nanocomposites. *Talanta* **2024**, *266*, 125037. [[CrossRef](#)] [[PubMed](#)]
114. Ostergaard, S.D.; Dinesen, P.T.; Foldager, L. Quantifying the value of markers in screening programmes. *Eur. J. Epidemiol.* **2010**, *25*, 151–154. [[CrossRef](#)] [[PubMed](#)]
115. Nielsen, D.M.; Ehm, M.G.; Weir, B.S. Detecting marker-disease association by testing for Hardy-Weinberg disequilibrium at a marker locus. *Am. J. Hum. Genet.* **1998**, *63*, 1531–1540. [[CrossRef](#)] [[PubMed](#)]
116. Kobayashi, T. A blood tumor marker combination assay produces high sensitivity and specificity for cancer according to the natural history. *Cancer Med.* **2018**, *7*, 549–556. [[CrossRef](#)] [[PubMed](#)]
117. Kokorina, A.A.; Ponomaryova, T.S.; Goryacheva, I.Y. Photoluminescence-based immunochemical methods for determination of C-reactive protein and procalcitonin. *Talanta* **2021**, *224*, 121837. [[CrossRef](#)] [[PubMed](#)]
118. Naik, A.; Yeong, J.; Decock, J. Editorial: Cancer testis antigens in cancer: Recent developments as cancer biomarkers and therapeutic targets. *Front. Oncol.* **2022**, *12*, 1075329. [[CrossRef](#)] [[PubMed](#)]
119. Quintero-Campos, P.; Segovia-de los Santos, P.; Ibanez-Echevarria, E.; de Rojas, D.H.-F.; Casino, P.; Lassabe, G.; Gonzalez-Sapienza, G.; Maquieira, A.; Morais, S. An ultra-sensitive homologous chemiluminescence immunoassay to tackle penicillin allergy. *Anal. Chim. Acta* **2022**, *1214*, 339940. [[CrossRef](#)]
120. Haji-Hashemi, H.; Norouzi, P.; Safarnejad, M.R.; Ganjali, M.R. Label-free electrochemical immunosensor for direct detection of Citrus Tristeza virus using modified gold electrode. *Sens. Actuators B Chem.* **2017**, *244*, 211–216. [[CrossRef](#)]
121. Zhang, X.; Shen, G.; Sun, S.; Shen, Y.; Zhang, C.; Xiao, A. Direct immobilization of antibodies on dialdehyde cellulose film for convenient construction of an electrochemical immunosensor. *Sens. Actuators B Chem.* **2014**, *200*, 304–309. [[CrossRef](#)]
122. Aydin, E.B.; Aydin, M.; Sezginurk, M.K. A label-free electrochemical biosensor for highly sensitive detection of GM2A based on gold nanoparticles/conducting amino-functionalized thiophene polymer layer. *Sens. Actuators B Chem.* **2023**, *392*, 134025. [[CrossRef](#)]
123. Zhao, C.; Wang, A.; Tang, X.; Qin, J. Electrochemical sensitive detection of amyloid- $\beta$  oligomer harnessing cellular prion protein on AuNPs embedded poly (pyrrole-3-carboxylic acid) matrix. *Mater. Today Adv.* **2022**, *14*, 100250. [[CrossRef](#)]
124. Taheri, N.; Khoshshafar, H.; Ghanei, M.; Ghazvini, A.; Bagheri, H. Dual-template rectangular nanotube molecularly imprinted polypyrrole for label-free impedimetric sensing of AFP and CEA as lung cancer biomarkers. *Talanta* **2022**, *239*, 123146. [[CrossRef](#)] [[PubMed](#)]
125. Kilic, T.; Gessner, I.; Cho, Y.K.; Jeong, N.; Quintana, J.; Weissleder, R.; Lee, H. Zwitterionic Polymer Electroplating Facilitates the Preparation of Electrode Surfaces for Biosensing. *Adv. Mater.* **2022**, *34*, 2107892. [[CrossRef](#)] [[PubMed](#)]
126. McIntyre, R.S.; Berk, M.; Brietzke, E.; Goldstein, B.I.; Lopez-Jaramillo, C.; Kessing, L.V.; Malhi, G.S.; Nierenberg, A.A.; Rosenblatt, J.D.; Majeed, A.; et al. Bipolar disorders. *Lancet* **2020**, *396*, 1841–1856. [[CrossRef](#)] [[PubMed](#)]
127. Chan, J.K.N.; Tong, C.H.Y.; Wong, C.S.M.; Chen, E.Y.H.; Chang, W.C. Life expectancy and years of potential life lost in bipolar disorder: Systematic review and meta-analysis (Feb, pg 1, 2022). *Br. J. Psychiatry* **2022**, *221*, 647–648. [[CrossRef](#)] [[PubMed](#)]
128. Sharma, V.; Doobay, M. Valproic acid-induced obsessive-compulsive disorder in a patient with bipolar disorder. *Bipolar Disord.* **2020**, *22*, 538–540. [[CrossRef](#)]
129. Felizardo, M.; Freitas, C. Valproic acid-induced hyperammonemic encephalopathy: A clinical case. *Eur. Psychiatry* **2022**, *65*, S728–S729. [[CrossRef](#)]
130. Yuan, Y.; Li, T.; Ye, Z.; Feng, Y.; Chen, Z.; Wang, Y.; Sun, Y.; Wu, H.; Yang, Z.; Wang, Y.; et al. A One-Step Electropolymerized Biomimetic Polypyrrole Membrane-Based Electrochemical Sensor for Selective Detection of Valproate. *Front. Bioeng. Biotechnol.* **2022**, *10*, 851692. [[CrossRef](#)]
131. Khairy, M.; Banks, C.E. A screen-printed electrochemical sensing platform surface modified with nanostructured ytterbium oxide nanoplates facilitating the electroanalytical sensing of the analgesic drugs acetaminophen and tramadol. *Microchim. Acta* **2020**, *187*, 1–10. [[CrossRef](#)] [[PubMed](#)]
132. Lagard, C.; Vodovar, D.; Chevillard, L.; Callebort, J.; Caille, F.; Pottier, G.; Liang, H.; Risede, P.; Tournier, N.; Megarbane, B. Investigation of the Mechanisms of Tramadol-Induced Seizures in Overdose in the Rat. *Pharmaceuticals* **2022**, *15*, 1254. [[CrossRef](#)] [[PubMed](#)]
133. Diouf, A.; Aghoutane, Y.; Burhan, H.; Sen, F.; Bouchikhi, B.; El Bari, N. Tramadol sensing in non-invasive biological fluids using a voltammetric electronic tongue and an electrochemical sensor based on biomimetic recognition. *Int. J. Pharm.* **2021**, *593*, 120114. [[CrossRef](#)] [[PubMed](#)]

134. Zhou, M.; Nie, W.; Qiao, L.; Huang, D.D.; Zhu, S.; Lou, S.; Wang, H.; Wang, Q.; Tao, S.; Sun, P.; et al. Elevated Formation of Particulate Nitrate From  $N_2O_5$  Hydrolysis in the Yangtze River Delta Region From 2011 to 2019. *Geophys. Res. Lett.* **2022**, *49*, e2021GL097393. [[CrossRef](#)]
135. Nestler, A.; Berglund, M.; Accoe, F.; Duta, S.; Xue, D.; Boeckx, P.; Taylor, P. Isotopes for improved management of nitrate pollution in aqueous resources: Review of surface water field studies. *Environ. Sci. Pollut. Res.* **2011**, *18*, 519–533. [[CrossRef](#)] [[PubMed](#)]
136. Morou-Bermudez, E.; Torres-Colon, J.E.; Bermudez, N.S.; Patel, R.P.; Joshipura, K.J. Pathways Linking Oral Bacteria, Nitric Oxide Metabolism, and Health. *J. Dent. Res.* **2022**, *101*, 623–631. [[CrossRef](#)] [[PubMed](#)]
137. Monser, L.; Sadok, S.; Greenway, G.M.; Shah, I.; Uglow, R.F. A simple simultaneous flow injection method based on phosphomolybdenum chemistry for nitrate and nitrite determinations in water and fish samples. *Talanta* **2002**, *57*, 511–518. [[CrossRef](#)] [[PubMed](#)]
138. Wang, L.; Wang, Q. Selective determination of nitrite/nitrate based on photo-induced redox activity of titanium dioxide. *J. Sep. Sci.* **2018**, *41*, 4075–4082. [[CrossRef](#)] [[PubMed](#)]
139. Zhang, L.; Wei, Z.; Liu, P. An all-solid-state  $NO_3^-$ -ion-selective electrode with gold nanoparticles solid contact layer and molecularly imprinted polymer membrane. *PLoS ONE* **2020**, *15*, e0240173. [[CrossRef](#)]
140. Pietrzak, K.; Wardak, C.; Malinowski, S. Application of polyaniline nanofibers for the construction of nitrate all-solid-state ion-selective electrodes. *Appl. Nanosci.* **2021**, *11*, 2823–2835. [[CrossRef](#)]
141. Motaghedifard, M.H.; Pourmortazavi, S.M.; Alibolandi, M.; Mirsadeghi, S. Au-modified organic/inorganic MWCNT/Cu/PANI hybrid nanocomposite electrode for electrochemical determination of nitrate ions. *Microchim. Acta* **2021**, *188*, 1–12. [[CrossRef](#)]
142. Ali, M.A.; Wang, X.; Chen, Y.; Jiao, Y.; Mahal, N.K.; Moru, S.; Castellano, M.J.; Schnable, J.C.; Schnable, P.S.; Dong, L. Continuous Monitoring of Soil Nitrate Using a Miniature Sensor with Poly(3-octyl-thiophene) and Molybdenum Disulfide Nanocomposite. *ACS Appl. Mater. Interfaces* **2019**, *11*, 29195–29206. [[CrossRef](#)]
143. Koshiha, Y.; Hirai, M.; Horike, S.; Fukushima, T.; Ishida, K. Preparation of poly(3,4-ethylenedioxythiophene) by vapor-phase polymerization at the interface between 3,4-ethylenedioxythiophene vapor and oxidant melt. *Mol. Cryst. Liq. Cryst.* **2019**, *688*, 53–59. [[CrossRef](#)]
144. Kohler, M.C.; Li, F.; Dong, Z.; Amineh, R.K. Real-Time Nitrate Ion Monitoring with Poly(3,4-ethylenedioxythiophene) (PEDOT) Materials. *Sensors* **2023**, *23*, 7627. [[CrossRef](#)] [[PubMed](#)]
145. Zhang, H.; Li, Y.; Zhang, Y.; Wu, J.; Li, S.; Li, L. A Disposable Electrochemical Sensor for Lead Ion Detection Based on In Situ Polymerization of Conductive Polypyrrole Coating. *J. Electron. Mater.* **2023**, *52*, 1819–1828. [[CrossRef](#)]
146. Xu, M.; Wang, X.; Liu, X. Detection of Heavy Metal Ions by Ratiometric Photoelectric Sensor. *J. Agric. Food Chem.* **2022**, *70*, 11468–11480. [[CrossRef](#)]
147. Xiao, L.; Zhao, Y.; Chang, G.; Yan, H.; Zou, R.; Zhang, X.; Wang, S.; He, H. A 3D phytic acid cross-linked high-porous conductive hydrogel integrating g-C $3N_4$  for electrochemical multiplex sensing of heavy metal ions. *Anal. Chim. Acta* **2023**, *1269*, 341341. [[CrossRef](#)] [[PubMed](#)]
148. Su, M.; Liu, Y.; Li, S.; Fang, Z.; He, B.; Zhang, Y.; Li, Y.; He, P. A rubber-like, underwater superoleophobic hydrogel for efficient oil/water separation. *Chem. Eng. J.* **2019**, *361*, 364–372. [[CrossRef](#)]
149. Kulkarni, B.B.; Suvina, V.; Balakrishna, R.G.; Nagaraju, D.H.; Jagadish, K. 1D GNR-PPy Composite for Remarkably Sensitive Detection of Heavy Metal Ions in Environmental Water\*\*. *ChemElectroChem* **2022**, *9*, e202101269. [[CrossRef](#)]
150. Alruwais, R.S.; Adeosun, W.A.; Marwani, H.M.; Jawaid, M.; Asiri, A.M.; Khan, A. Novel Aminosilane (APTES)-Grafted Polyaniline@Graphene Oxide (PANI-GO) Nanocomposite for Electrochemical Sensor. *Polymers* **2021**, *13*, 2562. [[CrossRef](#)]
151. Maheshwaran, M.; Sivaraman, G.; Kumar, K.K.S. An electrochemical voltammetric response of  $Hg^{2+}$  and  $Pb^{2+}$  ions using polyaniline-benzothiazole composite modified GCE electrode: Synthesis, characterization and quantum chemical calculation. *Microchem. J.* **2024**, *197*, 109865. [[CrossRef](#)]
152. Milikić, J.; Savić, M.; Janošević Ležaić, A.; Šljukić, B.; Ćirić-Marjanović, G. Electrochemical Sensing of Cadmium and Lead Ions in Water by MOF-5/PANI Composites. *Polymers* **2024**, *16*, 683. [[CrossRef](#)] [[PubMed](#)]
153. Abdulla, M.; Ali, A.; Jamal, R.; Bakri, T.; Wu, W.; Abdiryim, T. Electrochemical Sensor of Double-Thiol Linked PProDOT@Si Composite for Simultaneous Detection of Cd(II), Pb(II), and Hg(II). *Polymers* **2019**, *11*, 815. [[CrossRef](#)] [[PubMed](#)]
154. Curran, J.; Lo, J.; Leung, V.; Brown, K.; Schwartz, K.L.; Daneman, N.; Garber, G.; Wu, J.H.C.; Langford, B.J. Estimating daily antibiotic harms: An umbrella review with individual study meta-analysis. *Clin. Microbiol. Infect.* **2022**, *28*, 479–490. [[CrossRef](#)] [[PubMed](#)]
155. Kong, J.; Xu, X.; Ma, Y.; Miao, J.; Bian, X. Rapid and Sensitive Detection of Sulfamethizole Using a Reusable Molecularly Imprinted Electrochemical Sensor. *Foods* **2023**, *12*, 1693. [[CrossRef](#)] [[PubMed](#)]
156. Moghadam, M.R.; Salehi, L.; Jafari, S.; Nasirizadeh, N.; Ghasemi, J. Voltammetric sensing of oxacillin by using a screen-printed electrode modified with molecularly imprinted polyaniline, gold nanourchins and graphene oxide. *Microchim. Acta* **2019**, *186*, 1–7. [[CrossRef](#)]
157. Wu, D.H. Efficacy and tolerability of cefixime in otitis media. A multicentre study in over 25,000 children. *Drugs* **1991**, *42* (Suppl. S4), 30–32. [[CrossRef](#)] [[PubMed](#)]
158. Dehghani, M.; Nasirizadeh, N.; Yazdanshenas, M.E. Determination of cefixime using a novel electrochemical sensor produced with gold nanowires/graphene oxide/electropolymerized molecular imprinted polymer. *Mater. Sci. Eng. C Mater. Biol. Appl.* **2019**, *96*, 654–660. [[CrossRef](#)]

159. Zhou, T.; Yu, Z.; Zhang, L.; Gong, C.; Yan, C. Removal of sulfonamides from water by wetland plants: Performance, microbial response and mechanism. *Sci. Total Environ.* **2024**, *916*, 170181. [[CrossRef](#)]
160. Ribeiro, J.; Vieira, F.D.; King, T.; D'Arezzo, J.B.; Boyce, J.M. Misclassification of susceptible strains of *Staphylococcus aureus* as methicillin-resistant *S. aureus* By a rapid automated susceptibility testing system. *J. Clin. Microbiol.* **1999**, *37*, 1619–1620. [[CrossRef](#)]
161. Behera, K.; Mutharani, B.; Chang, Y.-H.; Kumari, M.; Chiu, F.-C. Protein-Aided Synthesis of Copper-Integrated Polyaniline Nanocomposite Encapsulated with Reduced Graphene Oxide for Highly Sensitive Electrochemical Detection of Dimetridazole in Real Samples. *Polymers* **2024**, *16*, 162. [[CrossRef](#)] [[PubMed](#)]
162. Silva, V.; Gai, L.; Harkes, P.; Tan, G.; Ritsema, C.J.; Alcon, F.; Contreras, J.; Abrantes, N.; Campos, I.; Baldi, I.; et al. Pesticide residues with hazard classifications relevant to non-target species including humans are omnipresent in the environment and farmer residences. *Environ. Int.* **2023**, *181*, 108280. [[CrossRef](#)] [[PubMed](#)]
163. Anirudhan, T.S.; Athira, V.S.; Nair, S.S. Detection of chlorpyrifos based on molecular imprinting with a conducting polythiophene copolymer loaded on multi-walled carbon nanotubes. *Food Chem.* **2022**, *381*, 132010. [[CrossRef](#)] [[PubMed](#)]
164. Ding, S.; Lyu, Z.; Li, S.; Ruan, X.; Fei, M.; Zhou, Y.; Niu, X.; Zhu, W.; Du, D.; Lin, Y. Molecularly imprinted polypyrrole nanotubes based electrochemical sensor for glyphosate detection. *Biosens. Bioelectron.* **2021**, *191*, 113434. [[CrossRef](#)] [[PubMed](#)]
165. Deller, A.E.; Hryniewicz, B.M.; Pesqueira, C.; Horta, R.P.; da Silva, B.J.G.; Weheabby, S.; Al-Hamry, A.; Kanoun, O.; Vidotti, M. PEDOT: PSS/AuNPs-Based Composite as Voltammetric Sensor for the Detection of Pirimicarb. *Polymers* **2023**, *15*, 739. [[CrossRef](#)] [[PubMed](#)]
166. Shu, L.; Mukherjee, M.; Wu, X. Toxic Gas Boundary Area Detection in Large-Scale Petrochemical Plants with Industrial Wireless Sensor Networks. *IEEE Commun. Mag.* **2016**, *54*, 22–28. [[CrossRef](#)]
167. Zhao, H.; Liu, L.; Lin, X.; Dai, J.; Liu, S.; Fei, T.; Zhang, T. Proton-Conductive Gas Sensor: A New Way to Realize Highly Selective Ammonia Detection for Analysis of Exhaled Human Breath. *ACS Sens.* **2020**, *5*, 346–352. [[CrossRef](#)] [[PubMed](#)]
168. Jain, A.; Nabeel, A.N.; Bhagwat, S.; Kumar, R.; Sharma, S.; Kozak, D.; Hunjet, A.; Kumar, A.; Singh, R. Fabrication of polypyrrole gas sensor for detection of NH<sub>3</sub> using an oxidizing agent and pyrrole combinations: Studies and characterizations. *Heliyon* **2023**, *9*, e17611. [[CrossRef](#)] [[PubMed](#)]
169. Park, E.; Kim, H.; Song, J.; Oh, H.; Song, H.; Jang, J. Synthesis of silver nanoparticles decorated polypyrrole nanotubes for antimicrobial application. *Macromol. Res.* **2012**, *20*, 1096–1101. [[CrossRef](#)]
170. Bhardwaj, S.K.; Mohanta, G.C.; Sharma, A.L.; Kim, K.-H.; Deep, A. A three-phase copper MOF-graphene-polyaniline composite for effective sensing of ammonia. *Anal. Chim. Acta* **2018**, *1043*, 89–97. [[CrossRef](#)]
171. Jiang, J.; Pi, Q.; Zhou, J.; Du, Y.; Li, Y. A simple preparation of ultrathin AuNWs-PEDOT:PSS bilayer Janus film for high performance chemiresistive ammonia gas sensor. *Sens. Actuators B Chem.* **2023**, *394*, 134370. [[CrossRef](#)]
172. Huang, Q.; Li, W.; Wu, T.; Ma, X.; Jiang, K.; Jin, X. Monoethanolamine-enabled electrochemical detection of H<sub>2</sub>S in a hydroxyl-functionalized ionic liquid. *Electrochem. Commun.* **2018**, *88*, 93–96. [[CrossRef](#)]
173. Bibi, A.; Santiago, K.S.S.; Yeh, J.-M.; Chen, H.-H. Valorization of Agricultural Waste as a Chemiresistor H<sub>2</sub>S-Gas Sensor: A Composite of Biodegradable-Electroactive Polyurethane-Urea and Activated-Carbon Composite Derived from Coconut-Shell Waste. *Polymers* **2023**, *15*, 685. [[CrossRef](#)] [[PubMed](#)]
174. Luo, K.-H.; Yan, M.; Hung, Y.-H.; Kuang, J.-Y.; Chang, H.-C.; Lai, Y.-J.; Yeh, J.-M. Polyaniline Composites Containing Eco-Friendly Biomass Carbon from Agricultural-Waste Coconut Husk for Enhancing Gas Sensor Performance in Hydrogen Sulfide Detection. *Polymers* **2023**, *15*, 4554. [[CrossRef](#)]
175. Ghosh, D.; Giri, S.; Mandal, A.; Das, C.K. H<sup>+</sup>, Fe<sup>3+</sup> codoped polyaniline/MWCNTs nanocomposite: Superior electrode material for supercapacitor application. *Appl. Surf. Sci.* **2013**, *276*, 120–128. [[CrossRef](#)]
176. Zhang, D.; Wang, D.; Zong, X.; Dong, G.; Zhang, Y. High-performance QCM humidity sensor based on graphene oxide/tin oxide/polyaniline ternary nanocomposite prepared by in-situ oxidative polymerization method. *Sens. Actuators B Chem.* **2018**, *262*, 531–541. [[CrossRef](#)]
177. Ansari, M.O.; Ansari, S.P.; Yadav, S.K.; Anwer, T.; Cho, M.H.; Mohammad, F. Ammonia vapor sensing and electrical properties of fibrous multi-walled carbon nanotube/polyaniline nanocomposites prepared in presence of cetyl-trimethylammonium bromide. *J. Ind. Eng. Chem.* **2014**, *20*, 2010–2017. [[CrossRef](#)]



178. Zhao, Z.; Ma, C.; Xu, L.; Yu, Z.; Wang, D.; Jiang, L.; Jiang, X.; Gao, G. Conductive Polyaniline-Based Microwire Arrays for SO<sub>2</sub> Gas Detection. *ACS Appl. Mater. Interfaces* **2023**, *15*, 38938–38945. [[CrossRef](#)]
179. Jang, D.; Jin, H.; Kim, M.; Park, Y.D. Polymeric interfacial engineering approach to perovskite-functionalized organic transistor-type gas sensors. *Chem. Eng. J.* **2023**, *473*, 145482. [[CrossRef](#)]

**Disclaimer/Publisher's Note:** The statements, opinions and data contained in all publications are solely those of the individual author(s) and contributor(s) and not of MDPI and/or the editor(s). MDPI and/or the editor(s) disclaim responsibility for any injury to people or property resulting from any ideas, methods, instructions or products referred to in the content.